Three-Dimensional Neutronics Analysis of the Mirrors-Beam Duct-Shield System for a Laser Driven Power Reactor

M.M.H. Ragheb, A.C. Klein, and C.W. Maynard

March 1978

UWFDM-239

FUSION TECHNOLOGY INSTITUTE

UNIVERSITY OF WISCONSIN

MADISON WISCONSIN

Three-Dimensional Neutronics Analysis of the Mirrors-Beam Duct-Shield System for a Laser Driven Power Reactor

M.M.H. Ragheb, A.C. Klein, and C.W. Maynard

Fusion Technology Institute
University of Wisconsin
1500 Engineering Drive
Madison, WI 53706

http://fti.neep.wisc.edu

March 1978

UWFDM-239

"LEGAL NOTICE"

"This work was prepared by the University of Wisconsin as an account of work sponsored by the Electric Power Research Institute, Inc. ("EPRI"). Neither EPRI, members of EPRI, the University of Wisconsin, nor any person acting on behalf of either:

"a. Makes any warranty or representation, express or implied, with respect to the accuracy, completeness, or usefulness of the information contained in this report, or that the use of any information, apparatus, method, or process disclosed in this report may not infringe privately owned rights; or

"b. Assumes any liabilities with respect to the use of, or for damages resulting from the use of, any information, apparatus, method or process disclosed in this report."

THREE DIMENSIONAL NEUTRONICS ANALYSIS OF THE MIRRORS-BEAM DUCT-SHIELD SYSTEM FOR A LASER DRIVEN POWER REACTOR

Magdi M.H. Ragheb
Andrew C. Klein
and
Charles W. Maynard

UWFDM-239

Fusion Research Program
Nuclear Engineering Department
The University of Wisconsin
Madison, Wisconsin, 53706, USA

TABLE OF CONTENTS

ABSTRACT

Monte Carlo three-dimensional neutronics calculations for the mirror and laser beam duct-shield system for a laser-driven power reactor are presented. The three section duct with right angle bends for the last two beam reflection and focusing mirrors, together with the associated lining and shielding, are analyzed. The study shows that a major design consideration in such designs will be the radiation leakage, not just the radiation damage to the last mirror as currently thought. The neutron leakage after the second beam reflection produces a flux of the order of 10^{10}n/(cm^2·sec) caused by the large size of the penetration. Even though less in magnitude than the flux at the end point of the neutral beam injectors in Tokamak designs, reported in the range of 10^{13}n/(cm^2·sec), it still leads to an inadmissible neutron dose rate of 10^6rem/hr after the second beam bend. The effect of material compositions on leakage is studied, as well as the neutron heating and radiation damage around the penetration. The neutron leakage is reduced by an order of magnitude when a Boral liner is used, instead of an aluminum one around the duct. The neutron heating rates and radiation damage parameters for the duct liner when Boral is used are of the same order as at the front of the last mirror and first wall, and will require a similar elaborate neutronic and mechanical design. Replacing the ordinary concrete duct shield by a Lead Mortar one does not ap-

preciably reduce the neutron leakage, which leads to the conclusion that the leakage in the system cannot solely be controlled by material compositions, but further gains must be obtained by modifying the geometrical configurations. Alternative shielding approaches for reducing the leakage are discussed. The afterheat and materials activations for a one-year reactor operation time are estimated for the mirrors and beam port lining.

ACKNOWLEDGEMENT

This research was partially suppported by a grant from the Electric Power Research Institute (EPRI). Thanks are due to Mrs. M. Emmert from ORNL, Dr. R. Conn, Dr. G. Kulcinski, Dr. W. Wolfer, Dr. W. Vogelsang, Dr. S. Abdel-Khalik, Dr. G. Moses, Dr. J. Howard, Dr. I. Sviatoslavsky, Dr. G. Cooper, Mr. M. Youssef, Mr. H. Avci from the Fusion Technology program, and Mr. R.J. Cashwell from the Reactor Laboratory at the University of Wisconsin for their help, discussions, and suggestions. Dr. E. Larsen from the Department of Chemistry and Mr. S. Sayegh from the Department of Nuclear Engineering, the University of Wisconsin provided data for the Lead Acetate Solution considered in the study. The excellent typing of Sherry Pomraning is greatly appreciated.

FIGURE CAPTIONS

Figure 1: Reactor Cavity Configuration. Vertical and Horizontal Sections.

Figure 2: Laser Beams Pellet-Illumination Geometry

Figure 3: Laser Beam Configurations for Different Turning Angles

Figure 4: Parabolic Mirror Geometry with 90° Turning Angle

Figure 5: Vertical Cut Through Water Cooled Laser Reactor Mirror

Figure 6: Mirror-Laser Beam Duct-Shield Configuration

Figure 7: Calculational Geometry Model

Figure 8: Space and Energy Dependences of the Neutron Scalar Flux

Figure 9: Specific Activity of Various Zones of the Last Mirror Versus Time

Figure 10: Specific Activity of Various Regions in Beam Port Liner Versus Time

Figure 11: Specific Afterheat of Various Zones Versus Time

Figure 12: Alternative Penetration Configurations

Figure A1: Coordinate System for Paraboloid of Revolution Mirror

Figure A2: Geometry of Off-axis Paraboloid of Revolution Mirror

LIST OF TABLES

I. INTRODUCTION

A Monte Carlo three-dimensional neutronics analysis for the mirror-laser beam duct-shield system for a conceptual laser-driven fusion power reactor design is presented. Detailed geometrical configurations including the reactor cavity, the two last mirrors and the three-section two-right-angle bends duct, are modelled. A current belief is that the main consideration in such designs is the radiation damage and heating to the last mirror. Our study suggests that an equally serious consideration is the radiation leakage from the system. The radiation damage problem to the last optical elements, and the ensuing loss of optical performance can be controlled, at least, by replacement. Radiation leakage, however, may lead to uncontrollable serious operational and safety problems. Due to the presence of bends, a neutron flux of 10^{10} $n/(cm^2 \cdot sec)$ is detected after the second mirror reflection and beam port bend, compared to a reported 10^{13} $n/(cm^2 \cdot sec)$ at the back of the neutral beam injectors in a Tokamak design [2]. Even though smaller in magnitude, this still leads to an inadmissible 10^6 rem/hr neutron radiation dose. This can be doubled by the presence of the secondary gammas generated by the neutron flux and by the activation radiation. The effect of the penetration shield materials compositions on neutron leakage is studied. Replacing the penetration Aluminum liner by a Boral one, succeeds in reducing it by an order of magnitude. Replacing the ordinary concrete shield by a Lead Mortar one fails to appreciably reduce the leakage further,

even though it is expected to appreciably reduce the gamma flux. The conclusion is that the leakage cannot be controlled merely by materials compositions, but further reduction must be obtained by alternative geometrical shielding configurations. Some suggestions are given and will require an iteration between the shielding and beam transport engineering. The penetration system is shown to require an elaborate cooling and replacement design, since the estimates of heating rates and radiation damage there are comparable to those occurring at the mirror front and at the first wall.

Ragheb, et al. [4] previously considered the gravity circulated Li_2O blanket concept for a laser-driven reactor which we also consider in this study. Discrete Ordinates and Monte Carlo calculational models for coupled neutron-gamma transport were compared in spherical geometry with respect to tritium breeding, neutron and gamma heating, and neutron primary damage effects in the reactor cavity. They assessed the application of Monte Carlo for one, two and three-dimensional scoping and design studies of the blanket system, and for the study of asymmetry effects, penetrations for multiple beam ducts, shielding of the cryogenic fuel-pellet injection and magnetic first wall protection systems. Ragheb, et al. [5,6] also considered an earlier version of the present design which consisted of a right circular cylinder with two hemispherical caps employing a magnetic protection of the cavity first wall. A two-dimensional Monte Carlo

study of the asymmetry effects in that design pointed out the difficulties such a reactor shape will lead to, with respect to heating and radiation damage nonuniformities and the consequent complex mechanical and heat transfer designs, and the varied component lifetimes. As a result of the latter study, alternative measures for the protection of the first wall were adopted, and a spherical reactor or cavity is now considered as shown in Figure 1. Ragheb, Gohar and Maynard [7] studied the choices of particle history termination parameters in Fusion Reactors scoping studies, and Ragheb and Maynard [9] also studied the choices of experiment-size parameters in such studies, by comparing one-dimensional Monte Carlo and Discrete Ordinate calculations. Recommendations from these studies are followed throughout the present work. A validation study of the version of the Monte Carlo code used in these calculations [12,13,14] was previously undertaken by Ragheb and Maynard [8] as a part of Monte Carlo three-dimensional cell calculations for a solid breeder gas cooled blanket design.

Previous Monte Carlo calculations of laser driven ICTR (Inertial Confinement Thermonuclear Reactors) blankets by other authors such as the early one-dimensional Booth [18] study, and the more recent two-dimensional one by Hansen and Maniscalco [11] and by Maniscalco, Meier and Monsler [36] did not consider the mirror-laser beam duct system; which is addressed in the present

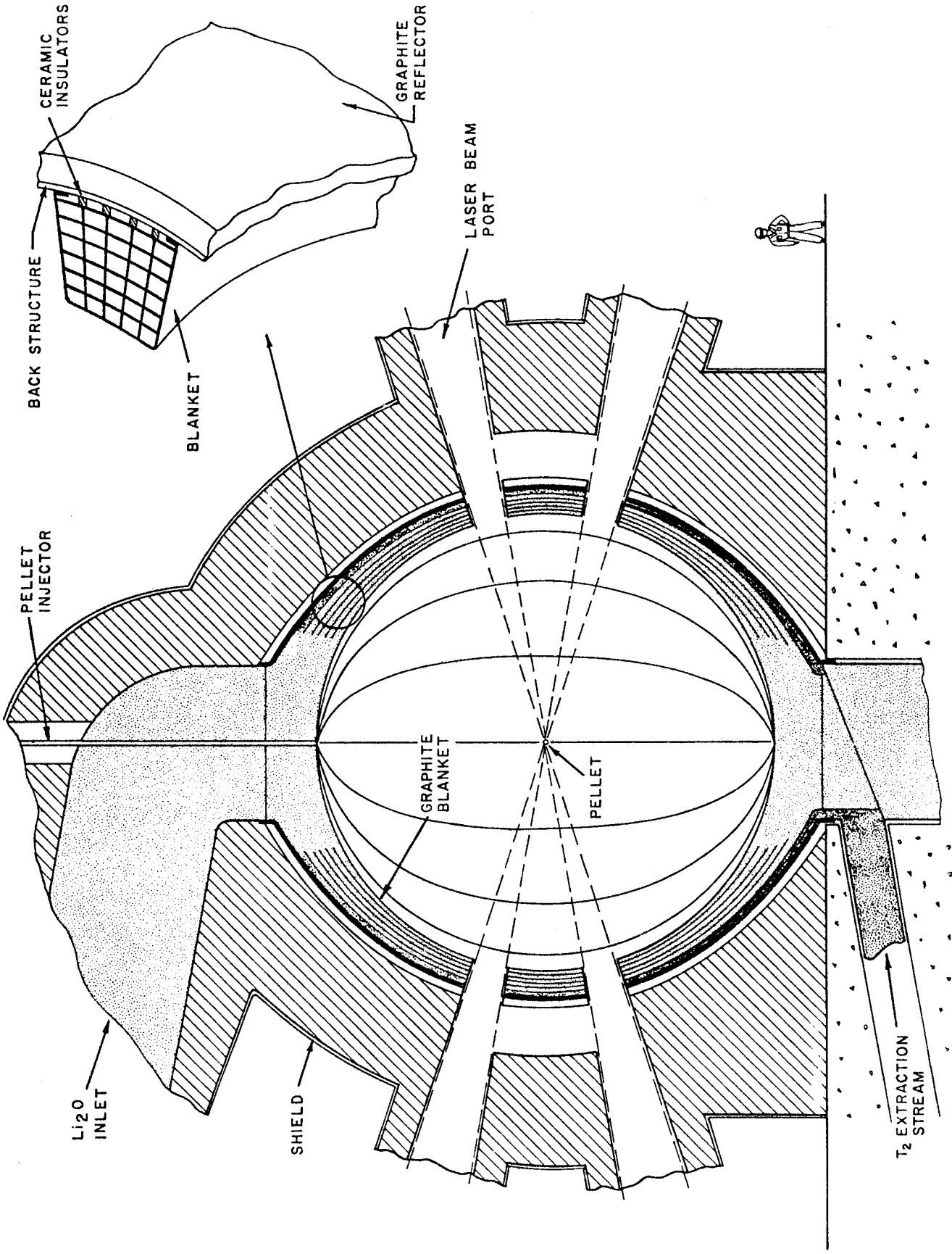
CERAMIC INSULATORS
GRAPHITE REFLECTOR
BACK STRUCTURE
BLANKET
LASER BEAM PORT
PELLET INJECTOR
GRAPHITE BLANKET
PELLET
Li_2O INLET
SHIELD
T_2 EXTRACTION STREAM

Figure 1.a

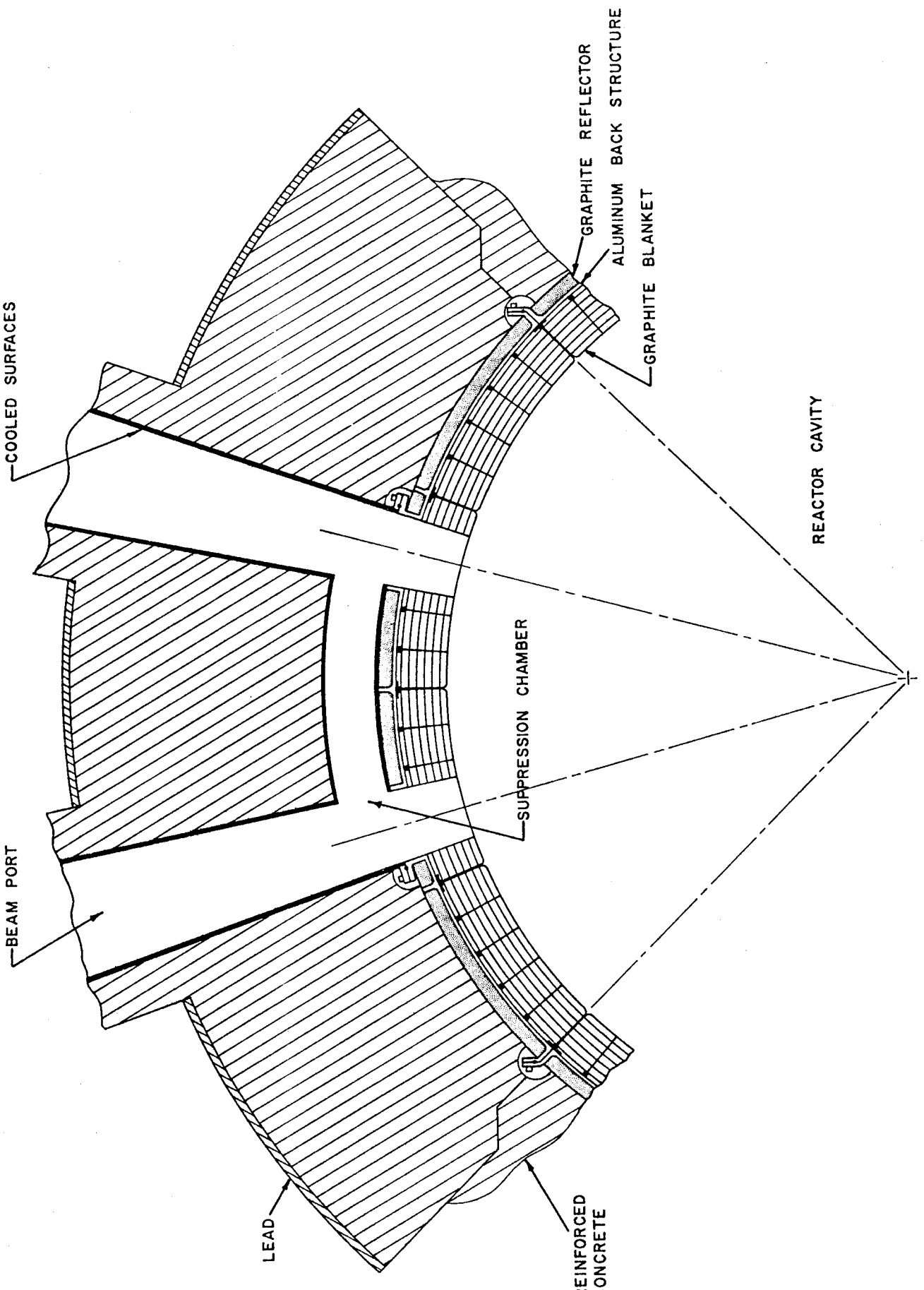
COOLED SURFACES
BEAM PORT
GRAPHITE REFLECTOR
ALUMINUM BACK STRUCTURE
GRAPHITE BLANKET
REACTOR CAVITY
SUPPRESSION CHAMBER
LEAD
REINFORCED CONCRETE

Figure 1.b

work. Ragheb and Maynard [10] have previously compared the neutron and gamma irradiation response of candidate materials for actively cooled laser fusion mirrors but did not treat the duct system.

Two-dimensional Discrete Ordinates methods have been used by Ide, Seki and Iida [1], as well as by Gohar and Maynard [19] to approximately model the effects of neutron streaming through neutral beam injection ducts in magnetic confinement Tokamak Reactors. Three-dimensional Monte Carlo has been used by Abdou, Milton, Jung and Gelbard [2] to calculate neutron flux distributions in the vicinity of simplified models of shielded penetrations in Tokamaks. Santoro, Tang, Alsmiller, Jr., and Barnes [3] used Adjoint Monte Carlo to estimate the nuclear heating and radiation damage at selected positions in the toroidal field coils of a Tokamak, adjacent to a rectangular neutral beam injector duct that passes through the blanket and shield. The problem considered here is of a quite different nature: on the one hand the shielding problem was thought to be easier than the one for neutral beam injectors since bends do exist in the beam penetration system, but on the other hand these bent geometrical configurations have a very large size and thus lead to an appreciable particle leakage. Moreover, they are quite difficult to model; so that here the calculations are largely man-hour consuming. Even though the detailed design of the mirror-laser beam transport

system must await the detailed design of the reactor cavity, it is found from this study that its impact is so great on the overall reactor design that it must be incorporated into it as early as possible to avoid conflicts between the energy removal, laser beam transport system, and shielding aspects of the design.

The calculational model and methods and the nuclear data used in the calculations are discussed in Sec. II. The results are presented and discussed in Sec. III, and suggestions for future investigations towards solving the problems uncovered by our study are presented in Sec. V. Section IV discusses the limitations of the used computational model.

II. DETAILS OF CALCULATIONS

II.1 Reactor Configuration

The Mirrors-Beam Duct-Shield system analysis depends on specific details of the reactor geometry. Here we consider the spherical geometry reactor of Figure 1. Lithium oxide serves as coolant and breeding material and flows gravitationally through a graphite compartmented blanket structure. Its flow is controlled by orificing. An ordinary concrete shield surrounds the blanket and its graphite reflector. Two clusters of six laser beams illuminate the pellet from two sides of the reactor cavity as shown in Figures 2 and 3. More details about the reactor configuration are given in References 20, 21, 37-40.

At a repetition rate of 20 Hz, a pellet yield of 150 MJ per pellet explosion is necessary to produce 3340 MW(th) [39] and a net electrical output of 1000 MW(e). The pellet design is such that its core at ignition consists of 1 mg of DT fuel at a compressed density-radius product (ρR) of 3 gm/cm^2, surrounded by 1.2 mg of high-Z material such as Xe or Hg. This pellet core will burn with a fractional burnup of 45%, and its gain of 150 suggests that an implosion efficiency of 10 to 20% is necessary [39]. The first wall and final mirror are protected from the x-ray and charged particle pellet debris by a Xenon fill gas at an average pressure of 1 Torr.

For a 17.62 Mev energy release per fusion event, the chosen repetition rate and pellet yield per explosion lead to a 14-Mev neutron source term of:

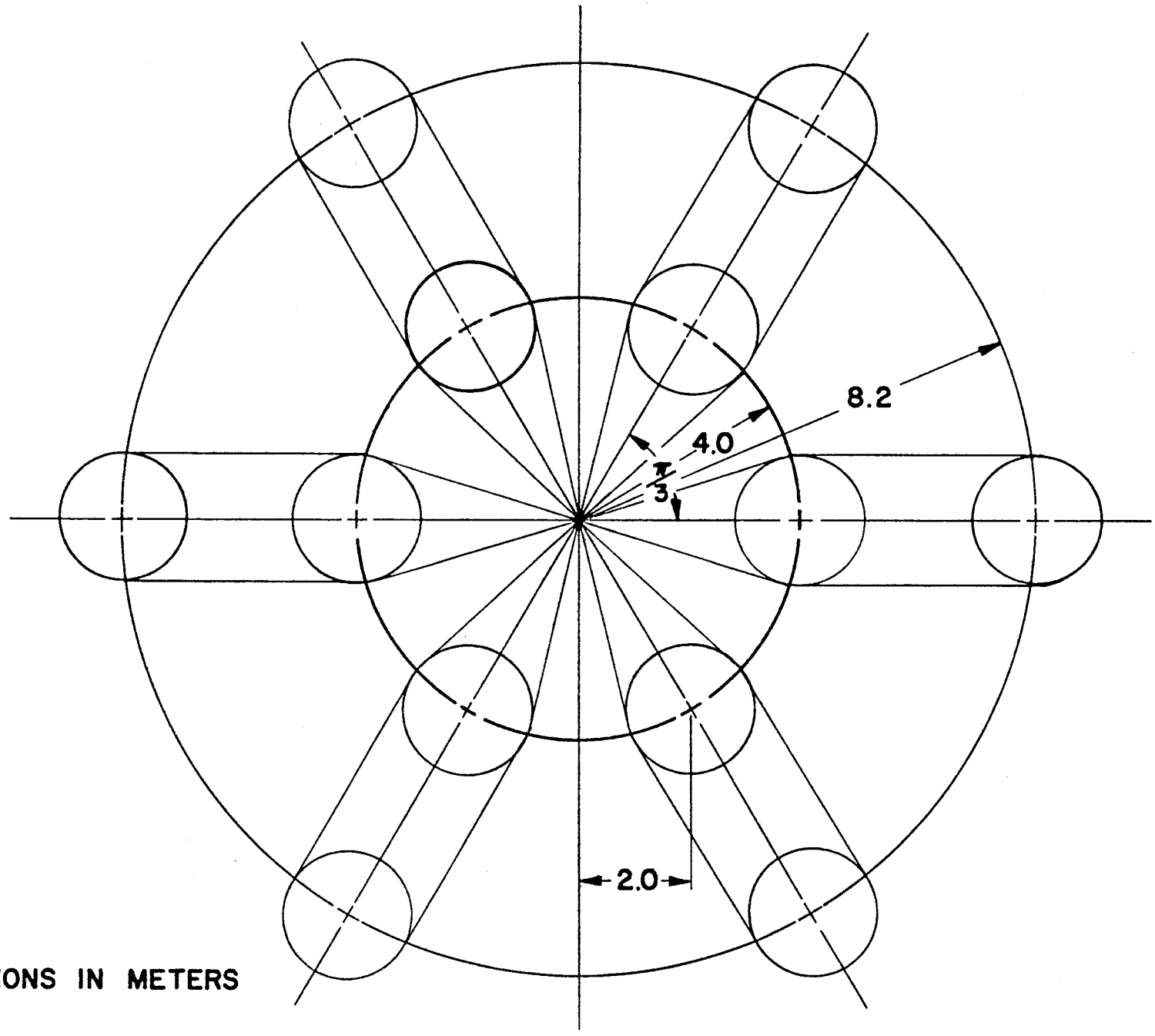

LASER BEAMS PELLET ILLUMINATION GEOMETRY

Figure 2

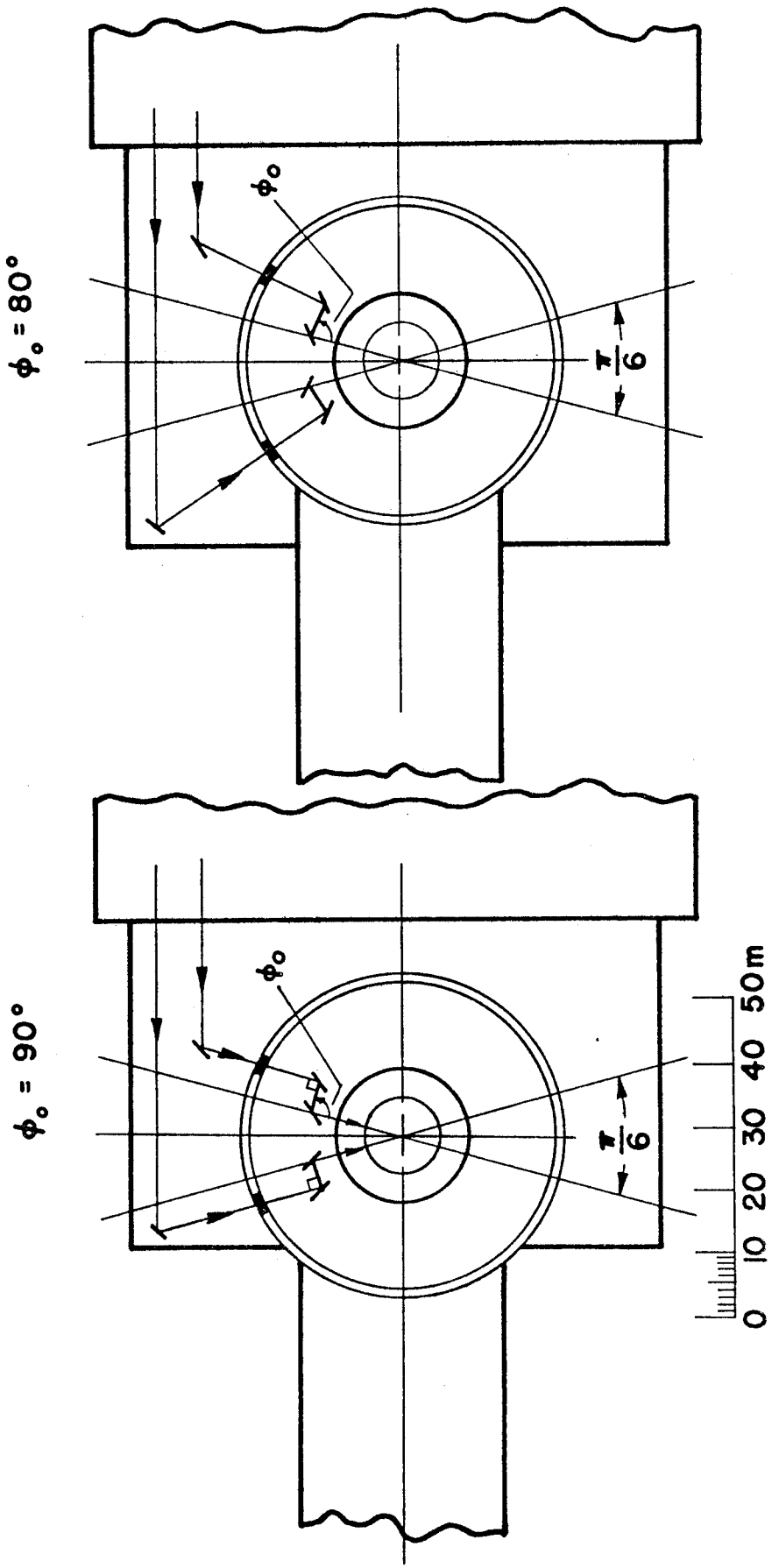

LASER BEAMS CONFIGURATIONS FOR DIFFERENT TURNING ANGLES

FIGURE 3

$$S = 150\ (MJ) \times 20\ (Hz) \times 10^{6}\ \left(\frac{Joules}{sec}\right) \times$$

$$\frac{1}{1.6021 \times 10^{-13}}\left(\frac{MeV}{Joules}\right) \times \frac{1}{17.62}\left(\frac{neutron}{Mev}\right)$$

$$= 1.063 \times 10^{21}\ [14\ MeV\ neutrons/sec]$$

II.2 Beam-Mirror Design Considerations

Reichelt et al. [17] discussed mirror materials constraints and choices, as well as fabrication techniques, and recommended the use of electroplated copper on aluminum as a mirror structural material. Copper base alloys and stainless steels, and low-expansion alloys such as Invar, are reported by Stark [16] as low-cost candidate structural materials for laser reactor mirrors. Ragheb and Maynard [10] studied the neutron and gamma irradiation response of water cooled mirrors for contemplated Laser Fusion Power Reactors for some candidate structural materials: Al, Cu, Ti, Mo and Fe. For a mirror located 15 m. from the reactor cavity center of 6 m. radius, their estimates for the neutron and gamma heating, atomic displacements and gas production rates were found to be one order of magnitude less than those occurring for fusion first-wall materials.

Off-axis parabolic mirrors, as used in this work, can be simultaneously used for turning and focusing a collimated laser beam. The diamond turning technique [16] makes their use more practical, although these mirrors have been difficult to fabri-

cate in the past. Howard [15] studied their imaging properties and recommended the use of turning angles less than or equal to $\pi/2$ to avoid distortions in the pellet illumination uniformity.

Figure 4 shows a parabolic mirror with a $\phi_o = 90°$ turning angle, as considered in this work, placed at a distance r_o from the center of a reactor cavity where Δt_s, Δt_r and Δt_b denote the thickness of the shield, reflector and blanket respectively. Relations pertinent to the mirror geometry are given in the Appendix.

The laser beam radius, r_B, is constrained by damage thresholds to at least 1 m [15].

The relationships A.1 to A.6 in the Appendix were used to compare different mirror choices A, B, C, and D as shown in Table I. We notice that ξ_1 and ξ_2 are not equal leading to imaging distortions as analyzed by Howard [15], but we do not pursue the point further here. The most important remark is that the subtended solid angle calculated by using the largest of either ξ_1 or ξ_2 in Equation A.7, decreases appreciably, for the same turning angle, when the mirror distance from the cavity center increases (Cases A, B and C). Keeping a small solid angle will decrease the radiation leakage from the reactor cavity, but will increase the plant cost since larger buildings and shielding requirements will still have to surround the remotely located mirrors. This may also lead to problems with respect to the beam positioning in

a vibrating reactor environment. It is also of interest to notice that the mirror size s is not very sensitive to the mirror location as shown in cases A, B and C, but is strongly sensitive to the turning angle ϕ_o as shown in cases B and D and in the table for case A. Decreasing the turning angle ϕ_o will in turn decrease the mirror sizes and consequently the subtended solid angle, but not as appreciably as by receding the mirror from the reactor cavity center. Different reactor configurations for different turning angles are shown in Figure 2. Thus the shielding requirement of keeping the solid angle as small as possible by emplacing the mirror as far as possible from the center of the reactor cavity, conflicts with the economics scaling which improves for a compact reactor and shield system size attainable by locating it as close as possible to the reactor cavity, within the limits of radiation damage and cooling requirements.

Based on the Ragheb and Maynard [10] study of the neutron and gamma irradiation response of uncoated laser reactor mirrors, a mirror with the dimensions of Figure 4 was chosen for further analysis. The radiation damage and heating requirements for a mirror emplaced at 15 m from the reactor center were thought manageable. The mirror dimensions and details are shown in Figure 5. It consists of two front and rear plates cooled by water circulating through square grooves, and connected by a

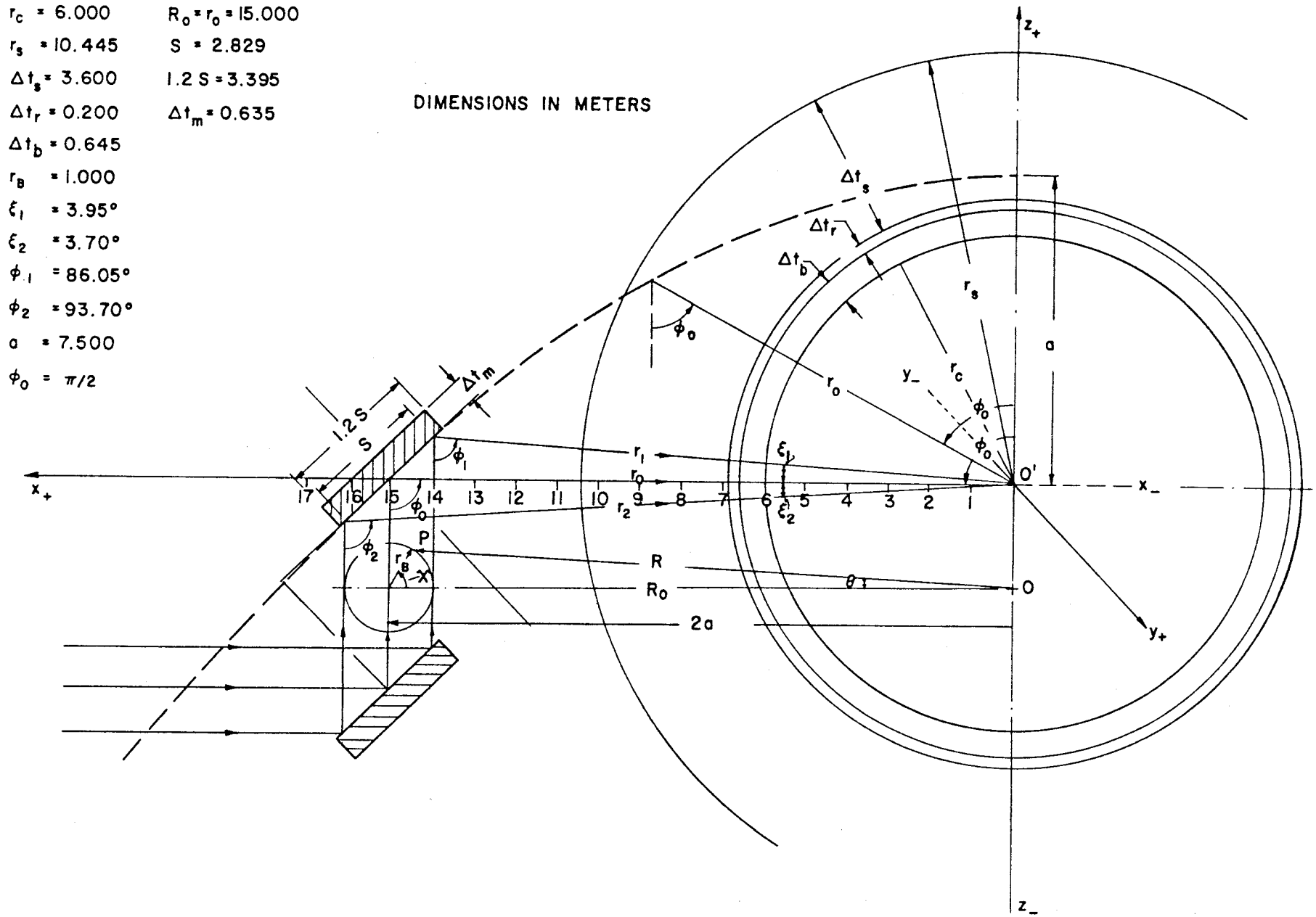

PARABOLIC MIRROR GEOMETRY WITH 90° TURNING ANGLE

Figure 4

honeycomb structure. The mirror is cylindrical in shape and has a radius of curvature of 42.43 m as shown in Table I (Case B). Such a curvature being very small, we modelled both the paraboloid and flat mirrors as right circular cylinders. The mirror structure is Aluminum, with an electroplated 1 mm thick layer of copper on the mirror front. The latter layer was not included in the neutronics calculations since being neutronically optically thin, it will not appreciably affect the neutron spectrum, but was included in activation calculations since copper activates substantially.

II.3 Mirror-beam Duct System Configuration

The flat and parabolic mirror system with the dimensions given in the last section and shown in Figure 5 was surrounded by the shielding shown in Figure 6. A 0.2 m clearance was left between the penetration wall and the beam edge. The penetration has been completely lined with a 0.635 cm liner. Spherical shields surround both the flat and paraboloid mirror. The solid angle shown was considered in the calculations. This models a single representative penetration for the beam cluster. For a conical half angle of 15°, the 14-MeV neutron source is (using Equation A.8):

$$S' = S \cdot \frac{d\Omega}{4\pi} = \frac{S}{2}[1 - \cos 15°]$$

$$= 1.81 \times 10^{19} \left[\frac{\text{14-MeV neutrons}}{\text{sec}}\right]$$

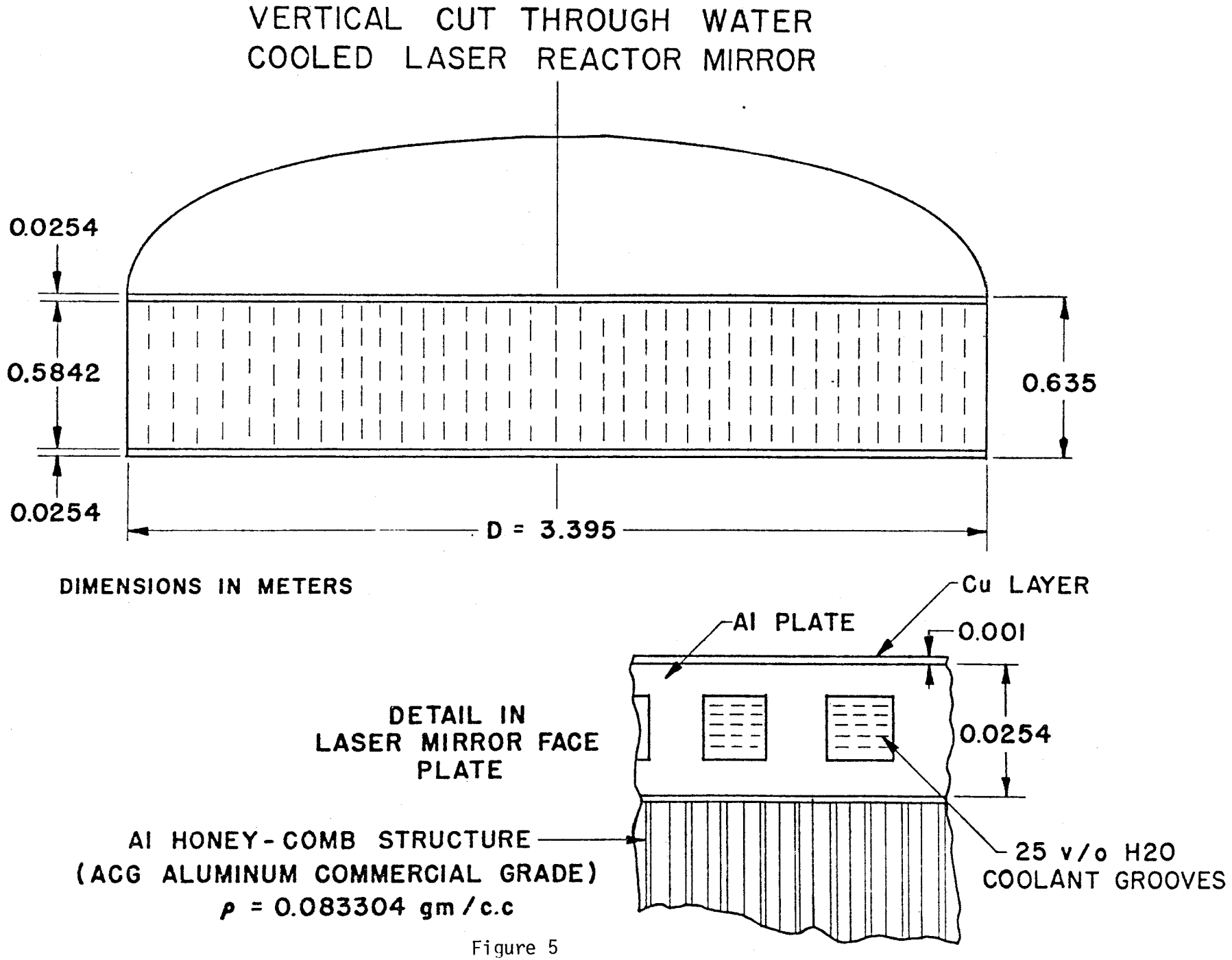
VERTICAL CUT THROUGH WATER
COOLED LASER REACTOR MIRROR
0.0254
0.5842
0.0254
0.635
D = 3.395
DIMENSIONS IN METERS
Cu LAYER
Al PLATE
0.001
DETAIL IN
LASER MIRROR FACE
PLATE
0.0254
Al HONEY-COMB STRUCTURE
(ACG ALUMINUM COMMERCIAL GRADE)
ρ = 0.083304 gm/c.c
25 v/o H2O
COOLANT GROOVES

Figure 5

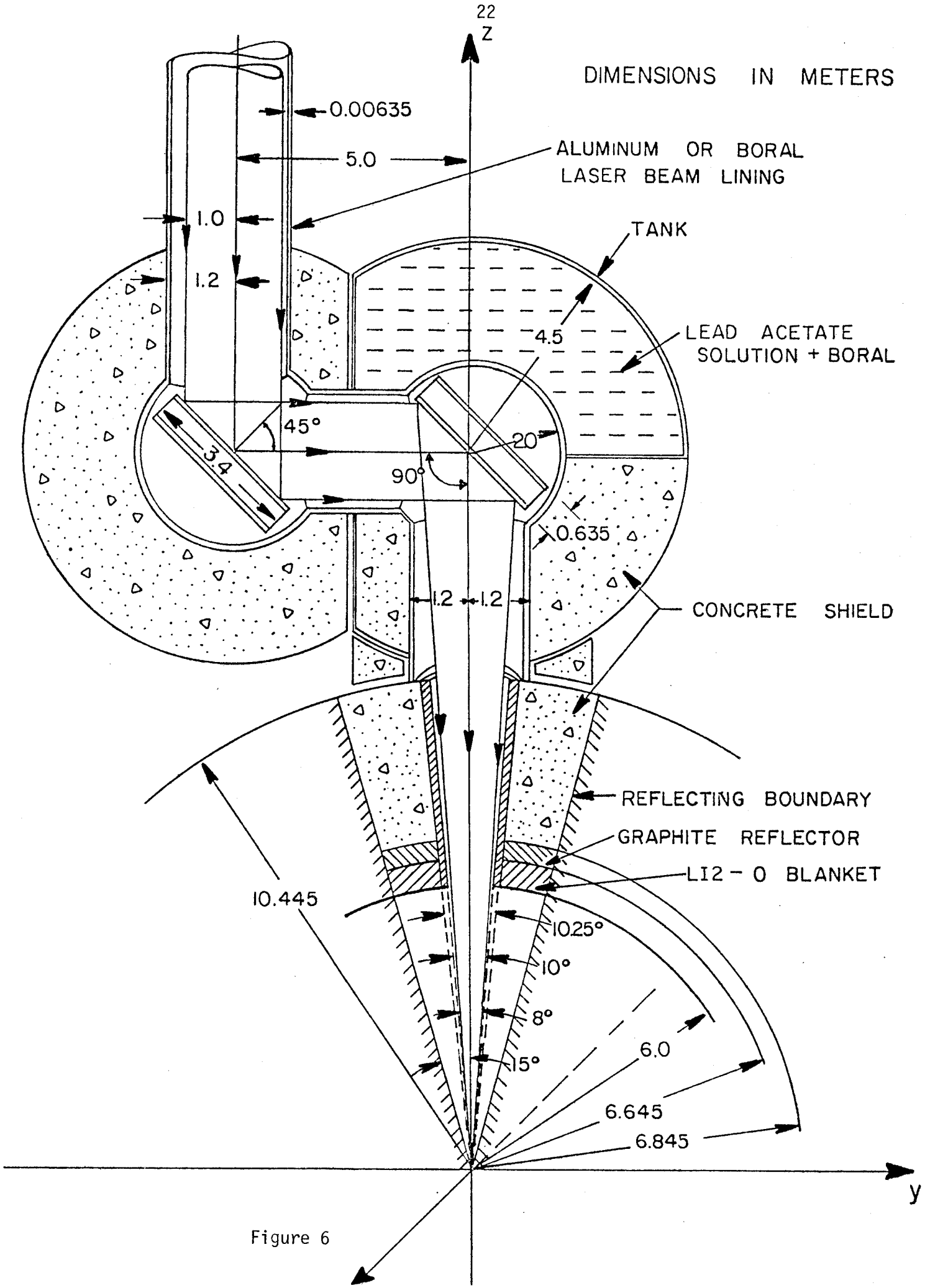
z
DIMENSIONS IN METERS
0.00635
5.0
ALUMINUM OR BORAL
LASER BEAM LINING
1.0
TANK
1.2
4.5
LEAD ACETATE
SOLUTION + BORAL
45°
20
3.4
90°
0.635
1.2
1.2
CONCRETE SHIELD
REFLECTING BOUNDARY
GRAPHITE REFLECTOR
LI2 - O BLANKET
10.445
10.25°
10°
8°
15°
6.0
6.645
6.845
y

Figure 6

where $S = 1.063 \times 10^{21}$ $[\frac{\text{14-MeV neutrons}}{\text{sec}}]$ which was used for the calculation of our time-integrated quantities. Normalization is to give 3,000 MW for the fusion power.

The conical-half angle of the duct lining through the reactor cavity was taken as 5° which is slightly greater than the laser-beam conical-half angle of 3.95° to allow a clearance between the laser beam and the duct wall. The neutron leakage from one single port can then be calculated as 2.031×10^{18} (14-MeV neutrons/sec) which corresponds to 4.56 (MW/beam) of leakage energy. For a total of 12 beams this is 54.66 (MW) of 14-MeV neutron energy leakage. Even though it is only 1.8 percent of the total 3000 MW fusion power, a 4.56 MW energy escape from each beam is quite appreciable. Ordinary concrete could not be used behind the last optical element because of the excessive heating resulting, and we choose a liquid shield of Lead Acetate in water, containing Boral sheets. Such a shield can be easily cooled, and will effectively shield against both neutrons and gammas. It actually acts as a secondary blanket, and by dumping the liquid from the containing tank, it can be easily removed for easy access to the last mirror for maintenance, adjustment or replacement. The rest of the shielding was initially taken as concrete, and later replaced by lead mortar. Space is not at a premium in our case as in the magnet shield of Tokamaks reactors, and the use of expensive minimum thickness exotic

shielding, such as tungsten or stainless steel used in other designs has been avoided in favor of economical minimum cost shielding. The last mirror nuclear design was such as to keep its optical thickness of the order of one mean free path for the 14-MeV neutrons, so as to allow a large fraction of them to just pass through it and start interacting with the tank wall and the Lead Acetate solution plus Boral. The Boral is included to absorb neutrons rather than letting them backscatter into the penetration. A liner of Aluminum or Boral is considered to cover the whole interior of the duct.

II.4 Material Compositions

Table II shows the materials and elemental compositions adopted in the study. The Aluminum structure and the water coolant in the front and rear of the mirror were homogenized. The honeycomb structure corresponds to ACG commercial grade Aluminum with a 0.083 gm/cm^3 density [35].

One of the interesting aspects of our study is the demonstration that the leakage can be reduced by an order of magnitude by use of a Boral liner instead of an Aluminum one. Such an idea can be adopted for Magnetic Confinement Penetrations as well. Boral is an Aluminum and B_4C mixture, clad in Aluminum. Boron Carbide (B_4C), is a dense, hard, highly inert material containing 80 percent Boron, and can be suspended in Aluminum up to 50 vol %. The resulting ingot can be rolled into sheets, aluminum

clad, and fabricated like aluminum. Boral with B_4C contents varying from 10 to 50 percent in the core can be supplied. Boron plates or sheets are usually supplied in standard sizes up to approximately 1 m by 3 m with standard thicknesses of 1/4 inch and 1/8 inch. We used the 1/4 inch thickness in our study. The heat conductivity of Boral is good; 0.432 W/cm°C at 90°C. The response to 14-MeV neutrons had not been addressed in the literature. Our present study provides calculated radiation damage responses and predicts a potential swelling problem caused by Helium and Hydrogen gas production.

The main advantages of Boron are high thermal neutron absorption, no penetrating gamma radiation and relatively low cost, as well as a large amount of available data. Irradiation response to fusion spectra is lacking, however, and requires extensive research. Its main disadvantage is the radiation damage due to neutron absorption. Gammas produced by neutron absorption are a major problem for shielding engineers; materials will absorb thermal neutrons but only by producing one or more 5 to 10-MeV secondary gammas that are a source requiring heat removal, and worse, further shielding. Boron is unique in its feature of readily absorbing thermal neutrons producing only a soft 1/2-MeV gamma and an easily absorbed alpha particle in the process, and leaving no significant induced residual radioactivity. Cadmium would emit several hard gammas and leaves four radioactive isotopes after neutron irradiation. Natural Boron has two isotopes

B-10 and B-11 with abundances 19.8 and 80.2% respectively. B-10 has an absorption cross section of 3838 barns at 0.025 ev, while that of B-11 is less than 0.05 barn. The cross section is 1/v in the region 0.01-100 ev. The reaction with thermal neutrons in an (n,α) reaction, the resulting Li^7 nucleus being stable. The reaction is accompanied by a 0.48 MeV gamma ray and 2.31 Mev in the form of kinetic energy, the latter being shared between the nucleus and the α-particle. Both particles are therefore ejected in opposite directions with high velocities so that they produce considerable ionization which leads to substantial radiation damage. Helium formation might produce swelling of the material. The 0.48 Mev gamma energy liberated is very small compared with that from Cadmium containing a spectrum with energies up to 9 Mev. Foreseeing the problem of heat generation and radiation damage in the Boral liner, we chose Boral with a reduced B_4C content of ~36 v/o.

Ordinary concrete (Type 3 Concrete from Reference 24) and Lead Mortar [25] were both considered as bulk and duct shield materials. The first was considered because of the absence of materials which can cause high activation, but was later dropped in favor of Lead Mortar (which corresponds to Chemtree product L6-82-5) because of its boron content for absorbing thermal neutrons, and its lead content for absorbing the secondary gammas.

The reactor blanket was considered as a homogenized mixture of graphite and lithium oxide.

A characteristic feature of our design is the lead acetate solution emplaced behind the last mirror for the reasons discussed in section II.3. The solubility of $Pb(C_2H_3O_2)_2$ in hot water is 221 gm/cm^3 [26]. It was experimentally found [21] that at a temperature of 50°C, 221 gm of lead acetate dissolved in 100 cm^3 of H_2O produces 154 cm^3 of the solution, from which our nuclides densities were calculated. Five v/o of Boral is added as sheets in the solution to absorb neutrons, supplementing the absorbing action of lead to the generated gamma rays.

II.5 Cross Section Data

The elements used in the calculations together with their atomic densities are shown in Table II.

The multigroup neutron cross sections were used in the structure shown in Table III. Table IV shows the identifications of the elements used. A P3 scattering anisotropy was used. The transport cross sections were taken from the coupled 100n - 21γ group cross section library prepared for EPR calculations [28,29] and designated as DLC-37B by the Radiation Shielding Information Center [27]. These were compiled from the ENDF/B-IV data file. The GAM-II [33] six first groups are kept the same, as well as the thermal group, and the intermediate groups were collapsed according to the group structure shown. Energy deposition was estimated with group-collapsed neutron kerma factors obtained from the work by Abdou and Roussin [30]; as well as the

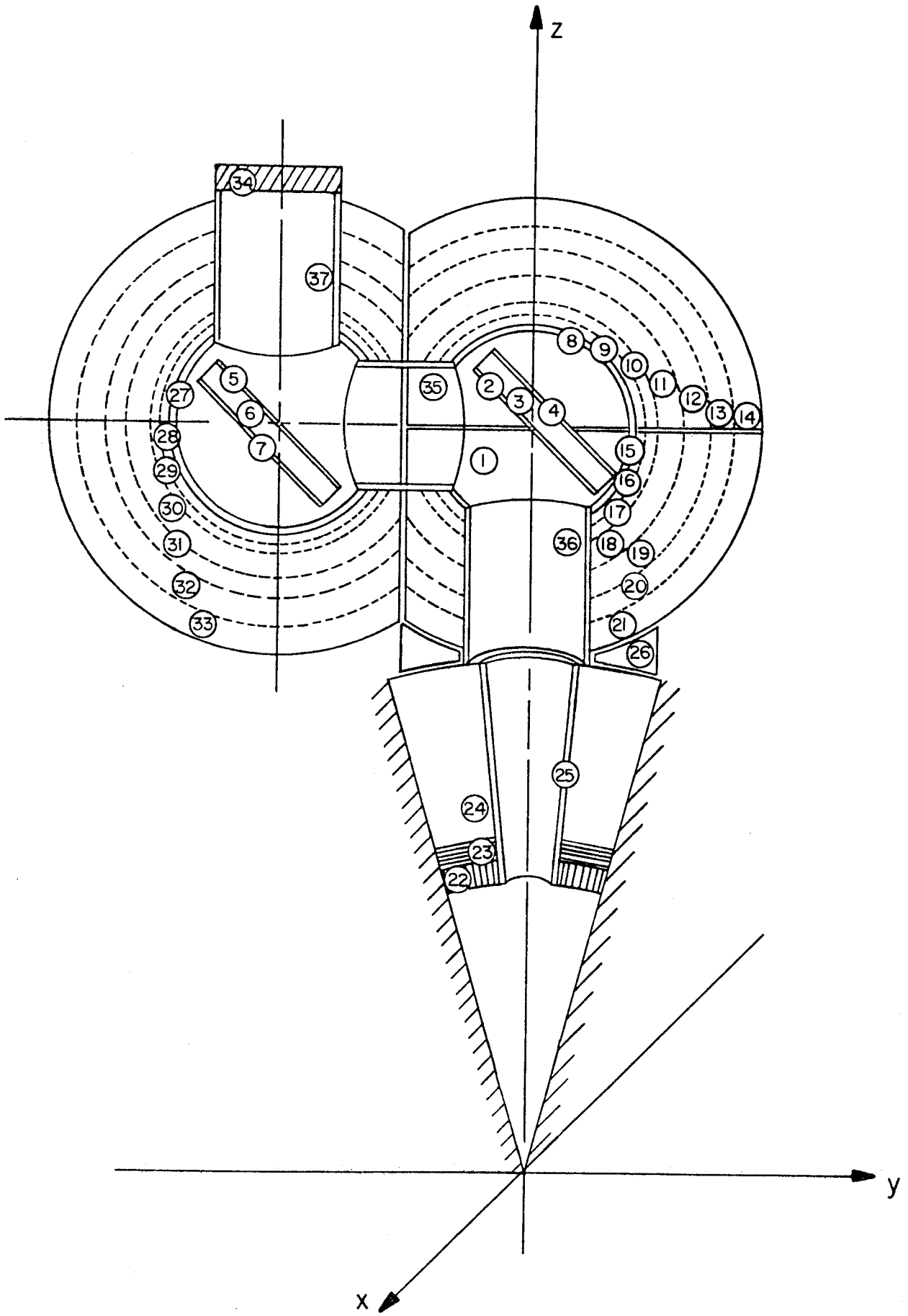
z
y
x
1
2
3
4
5
6
7
8
9
10
11
12
13
14
15
16
17
18
19
20
21
22
23
24
25
26
27
28
29
30
31
32
33
34
35
36
37

Figure 7

gas-production cross sections. The atomic displacement cross sections were adopted from the work of Avci and Kulcinski [31], in turn based on the work of Gabriel, Auburgey and Greene [32]. Whereas the data of References 31 and 32 are based on the ENDF/B-IV point cross section data, those of Reference [30] were based on ENDF/B-II data and need updating. The flux-to-dose conversion ratios of Table III were adopted from the work of Courtney [34].

II.6 Calculational Model

The beam-penetration reactor cavity system shown in Figures 1 and 6 is modelled in detail as shown in Figure 7 and Table V. The geometry is divided into 37 detector regions with the dimensions shown. Regions 2, 4, 5, 7 are a homogenized mixture of Al and H_2O representing the front and rear of the mirrors. Regions 3 and 6 model the honeycomb structure of the mirrors. The beam penetration is lined with a 0.635 cm thick liner of either Aluminum or Boral modelled by regions 8, 15, 25, 27, 35, 36 and 37. Regions 22, 23, and 24 model the reactor cavity blanket, reflector and shield respectively. The neutron source was sampled within the shown solid angle of 15° conical half angle; and is surrounded by a conical albedo surface. The lead acetate plus Boral shield is divided into 6 spherical shell regions. The same applies to the ordinary concrete or lead mortar shields. To quantify the neutron leakage after the second mirror, an end

cap composed of SiO_2 (Natural Quartz) was emplaced at the outlet of the beam penetration after the flat mirror shield.

In our study we needed estimates of integrated values over the regions shown, and there was no need for detailed flux distributions at each point. This kept the cost of calculations low. This is one of the advantages of the Monte Carlo method in that it can be "tailored" to the needs of the investigator both with regards to the information he needs, and to his budgetary limitations.

In our calculations, the collision estimator was used in conjunction with region detectors to estimate reactions of interest in the form

$$F_v = \langle \Sigma_{rv}(E_k), \bar{\psi}_v(E_k) \rangle \quad [\frac{\text{interactions}}{\text{source particle}}] \qquad (1)$$

where: $\Sigma_{rv}(E_k) = \sum_{i=1}^{s} N_{vi}\sigma_i(E_k)$, is a response function of interest $[cm^{-1}]$ in region v, for group E_k

N_{vi} is the nuclide number density of the considered element i in an alloy or mixture of s elements in [atoms/(barn·cm)], in detector region v.

$\sigma_i(E_k)$ is the microscopic cross section of the reaction of interest for element i [barns] and energy group E_k.

v designates the region detector of interest

$$\bar{\psi}_v(E_k) = \frac{1}{\sum_{Tv}(E_k)} \frac{\sum_{j=1}^{n_{vi}} W_j(E_k)}{n_t} \left[\frac{\text{interaction} \cdot \text{cm}}{\text{source particle}}\right]$$

is the volume-integrated fluence for energy group E_k

n_t is the total number of source particles

n_{vi} is the number of particles of energy E_i scattering in region v

$W_j(E_k)$ is the weight of the j-th particle at energy E_k scattering in region v.

$\sum_{Tv}(E_k)$ is the total macroscopic cross section for group E_k in region v $[cm^{-1}]$

G is the number of groups treated

$< , >$ denotes an inner product over the energy groups k = 1, 2,...,G

For the estimation of the design quantities of interest renormalization of the estimates is necessary to avoid numerical overflow during the calculations. For the estimation of particle fluxes, the response function $\sum_{rv}(E_k)$ in Equation 1 is input as a step function in the energy groups and regions of interest, renormalized by the source term and the region volumes, to obtain the volume integrated particle fluxes from the estimate:

$$\Phi_v = < \sum_{fv}(E_k), \bar{\psi}_v(E_k) > \left[\frac{\text{particles}}{cm^2 \cdot sec}\right] \qquad (2)$$

where: $\sum_{fv}(E_k) = \frac{S'}{V_v}$

S' is the source term, and is equal to the 4π source term multiplied by $\frac{\Omega}{4\pi}$, where Ω is the solid angle in which the source is sampled

In the cases studied here, $S' = 1.811 \times 10^{19}$ $[\frac{\text{source neutrons}}{\text{sec}}]$

V_v is the volume of region detector v, $[cm^3]$.

As an input to the thermal and hydraulic calculations, the neutron heating per source particle is estimated from:

$$H_v = \langle \sum_{Hv}(E_k), \bar{\psi}_v(E_k) \rangle \; [\frac{\text{ev}}{\text{source particle}}] \qquad (3)$$

where: $\sum_{Hv}(E_k) = \sum_{i=1}^{S} N_{vi} K_i(E_k)$ is the heating response function $[ev \cdot cm^{-1}]$ in region v,

$K_i(E_k)$ is the Kerma factor in energy group k [barn·ev], for element i.

To get the average volumetric heating rates in region v one uses:

$$Q_v = \langle \sum_{Qv}(E_k), \bar{\psi}_v(E_k) \rangle \; [\frac{\text{Watts}}{cm^3}] \qquad (4)$$

where: $\sum_{Qv}(E_k) = \frac{S'}{V_v} \cdot C_Q \cdot \sum_{Hv}(E_k)$

$C_Q =$ 1.6021×10^{-19}, is a conversion factor from ev to Joule.

As an input to the materials calculations, the gas production rates are estimated from:

$$G_v = \langle \sum_{Gv}(E_k), \bar{\psi}_v(E_k) \rangle \; [\frac{\text{appm}}{\text{sec}}] \qquad (5)$$

where: $\Sigma_{Gv}(E_k) = \frac{S' \cdot 10^{-18}}{V_v} \cdot \left[\sum_{i=1}^{S} N_{vi} \cdot \sigma_{Gi}(E_k) \right] \Big/ \sum_{i=1}^{S} N_{vi}$

For Hydrogen gas production: $\sigma_{Gi}(E_k) = \sigma_i(n,p) + \sigma_i(n,D) + \sigma_i(n,T) + \ldots$

For Helium gas production: $\sigma_{Gi}(E_k) = \sigma_i(n,HE\text{-}3) + \sigma_i(n,HE\text{-}4) + \ldots$

The atomic displacement rates are estimated from:

$$D_v = \langle \Sigma_{Dv}(E_k), \bar{\psi}_v(E_k) \rangle \quad [\frac{\text{displacement}}{\text{atom} \cdot \text{sec}}] \qquad (6)$$

where: $\Sigma_{Dv}(E_k) = \frac{S' \cdot 10^{-24}}{V_v} \cdot \nu_D(E_k) N_v \cdot \sigma_{vpk}(E_k)$

$\nu_D(E_k)$ is the number of displacements per primary knock-on of energy E_k

$\sigma_{vpk}(E_k)$ is the primary knock-on cross section from radiation damage theory [barns]

N_v is the atomic density of the metal matrix, in atoms/(barn·cm)

Since our primary interest was radiation leakage and the interactions around the penetration itself and not the detailed design of the shield, particles were followed in detail around the penetration, but those that penetrated deep and suffered many collisions in the shields were not followed in the simulation. The Russian Roulette routines in the computer code were modified so as to consider two types of regions:

i) Important regions, where the Russian Roulette is carried out the normal way. These were the liner regions and regions directly adjacent to them. In Case III

(Table XII), the Russian Roulette triggering weight was 10^{-9} and the survival probability was 90%.

ii) Less important regions, where the survival probability of particles undergoing Russian Roulette after falling below the Russian Roulette triggering weight, is zero. This amounts to the physical argument that particles getting deep into the shield and falling below a certain weight are very unlikely to scatter back to the penetration, which is our primary interest. Mathematically, this amounts to truncating the Neumann series solution at some high order. In Case III (Table XII), this modified procedure triggering weight was 10^{-5} in the shield and reactor cavity regions.

Thus the right particle reflection from the penetration walls is obtained, without wasting computation time following neutrons which will not contribute to the quantities of interest.

Results of the calculations are discussed in the following section.

III. DISCUSSION OF RESULTS

III.1 Scalar Flux Space and Energy Distributions:

Table XII shows the statistics of three cases. Cases I and II consider ordinary concrete as shield material and Case III, a lead mortar shield. Case I considered aluminum as the port lining, and Cases II and III considered it to be Boral. Notice that very low computation costs were involved, and it yielded the information needed for the scoping studies we are carrying out without recourse to the use of a very large number of histories.

Table VI shows how Boral is superior to aluminum as a duct liner. In the vacuum region, and the faces of both mirrors, the number of neutron tracks for the thermal-group neutrons are drastically reduced in the Boral case since Boron is a strong thermal-neutron absorber. However, the intermediate energy groups are not as strongly affected. Our study suggests Boral as an effective candidate duct lining material for both inertial and magnetic confinement fusion reactor penetrations.

Table VII compares the total and thermal-group fluxes in different reactor components for the three cases studied. At the parabolic mirror the thermal neutron flux is highly reduced in the Boral case, but not as much reduction is obtained in the lead mortar case. The total flux is about the same since it is mostly composed of fast neutron components as can be inferred

from Table VIII for Case III. At the flat mirror, both the total and thermal-group fluxes are reduced by the use of Boral. In that case the flux is mostly in intermediate energy groups as shown in Table VI. The thermal group is knocked out in the case of Boral. No 14-Mev neutrons reach the flat mirror as shown in Table VIII. In all three cases the fast flux at the paraboloid mirror front is less than at the blanket by the $1/R^2$ factor and the $1/\cos\theta$ factor, where θ is the angle of mirror tilt. However the thermal-group flux is higher than in the blanket by an order of magnitude due to the reflection from the lead acetate tank. The total flux is only an order of magnitude less than in the blanket.

At the reactor cavity shield and the ring shield around the duct, lead mortar gives a better attenuation than ordinary concrete. A comparison of the properties of different shielding concrete and mortar materials in fusion spectra with respect to cost, attenuation of neutrons and gammas, heating rates and charged particle production is needed. Some data on these aspects for ordinary concrete and lead mortar are obtained in the present study. Lead mortar attenuates thermal-group neutrons in zone 3 of the paraboloid mirror shield three orders of magnitude more than ordinary concrete because of the presence of boron; but the total flux is less by only an order of magnitude.

Around the penetration lining the thermal group is reduced by two to three orders of magnitude when Boral is used instead

of Aluminum as a duct liner. A further order of magnitude is noticed in some regions from the use of lead mortar. However, the thermal neutrons are the ones most affected, since the total flux is reduced by an order of magnitude in the case of Boral, and is only about halved when lead mortar is used. The conclusion is that the Boral and the lead mortar can control the thermal-group neutrons, but the intermediate energy neutrons still are able to leak out of the duct because of its large size. Further control of the leakage requires alternative geometrical configurations as suggested in Section V.

Table VIII lists the thermal, 14-Mev and total fluxes for Case III. The fractional standard deviation in the estimates of fluxes is shown and applied to the other estimated quantities. It can be noticed that some regions like the flat mirror and its shield and parts of the duct lining do not receive any 14-Mev neutrons for 8000 history simulations.

Figure 8 shows the space and energy dependences of the neutron scalar flux around the penetration in the liner for the case of Boral as the liner and lead acetate as the shield. Note that the lead acetate tank wall behind the last mirror is affected by larger 14-Mev and thermal group fluxes than the reactor cavity liner. Thus the same design requirements as for the reactor blanket may have to be adopted there. The effect of Boral is to eliminate the thermal flux component in regions of the duct af-

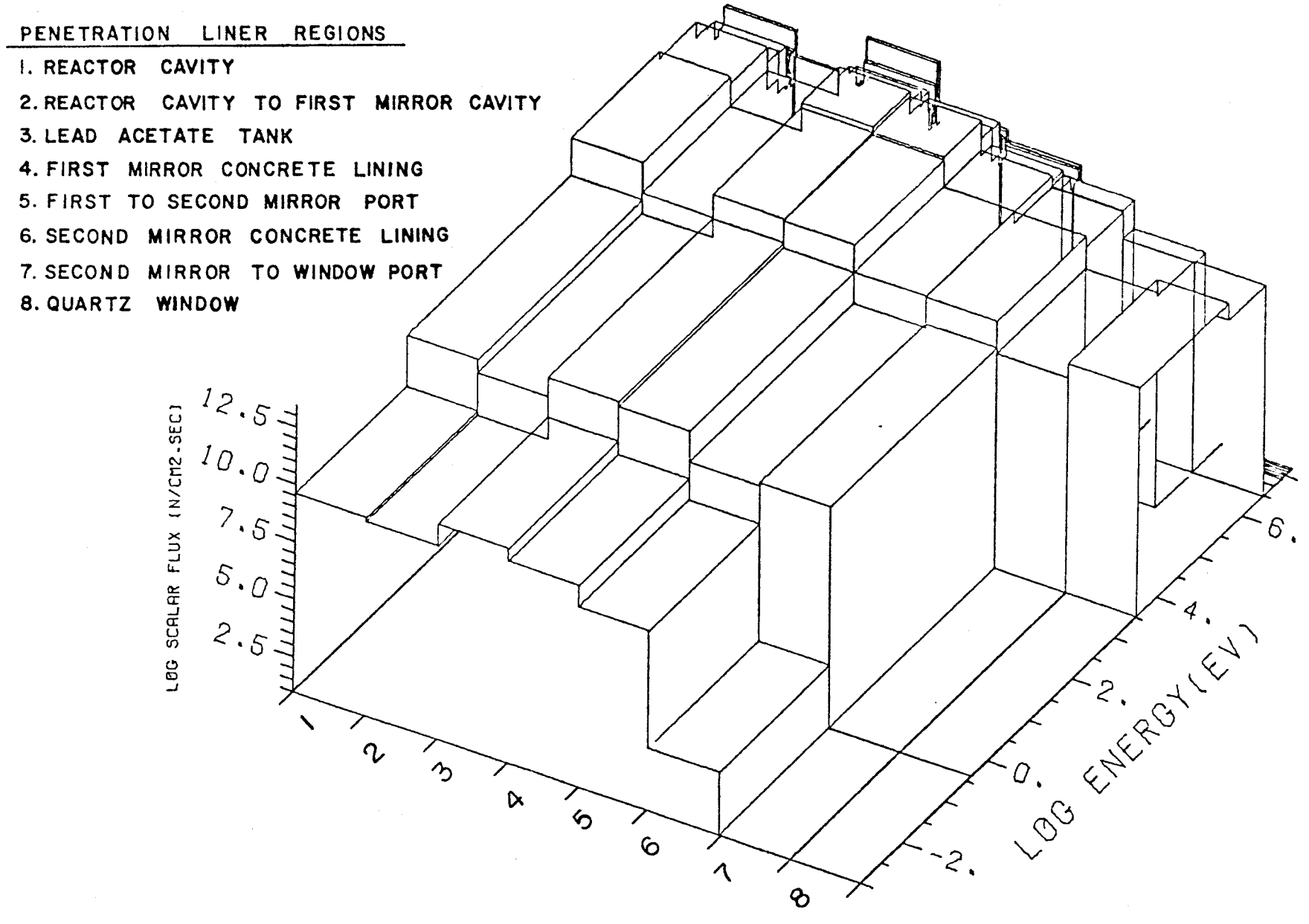

SPACE AND ENERGY DEPENDENCES OF THE NEUTRON SCALAR FLUX

Figure 8.a

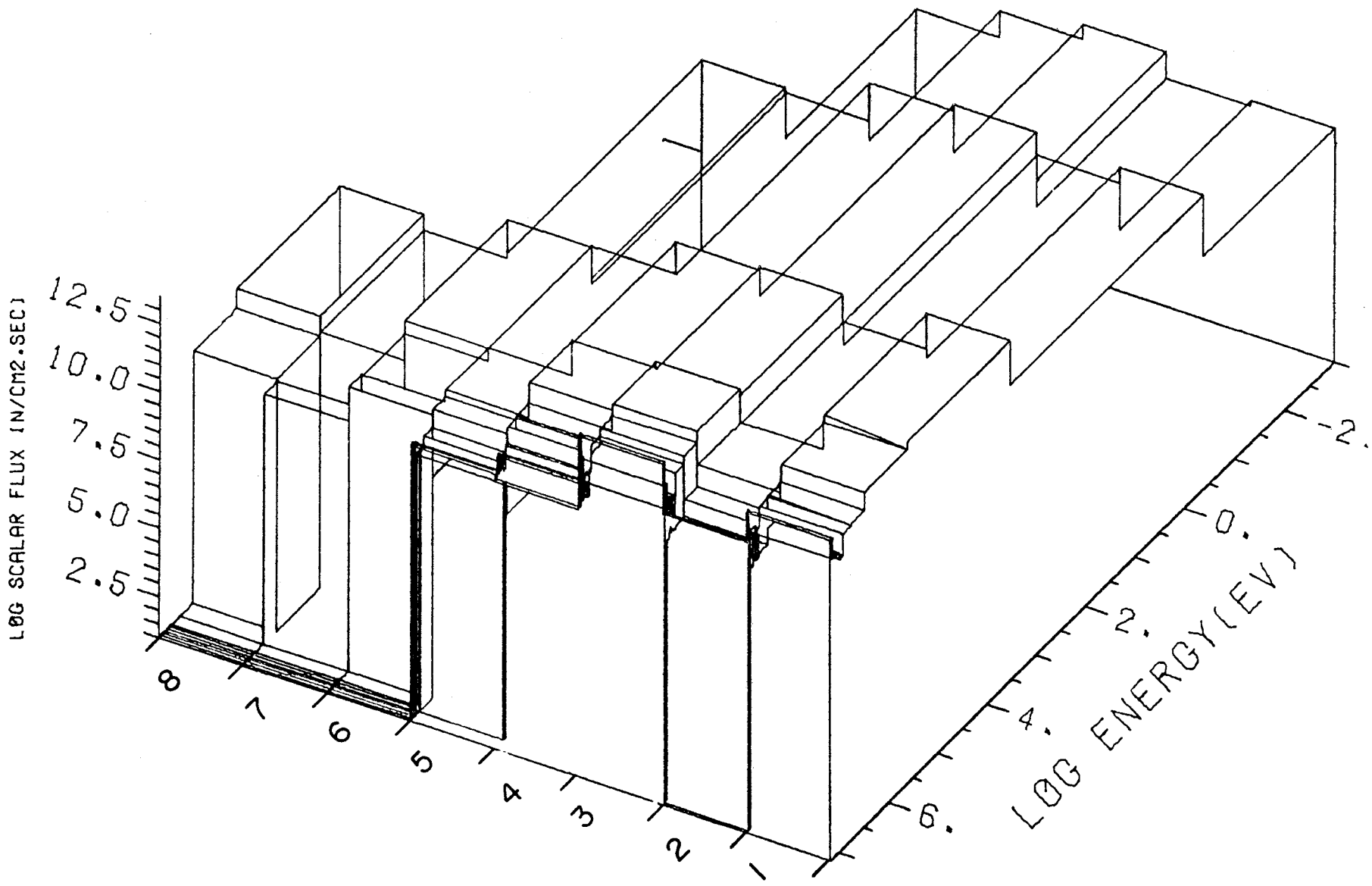

SPACE AND ENERGY DEPENDENCES OF THE NEUTRON SCALAR FLUX

Figure 8.b

ter the second mirror. The high energy group components are also eliminated. However, some intermediate energy particles are able to leak there in the kev and Mev regions. These are particles which suffered few collisions with the walls of the penetration and are able to leak because of its relatively large size.

III.2 Nuclear Heating and Dose Rates:

Table IX shows the volumetric neutron heating rates in the different reactor regions. The parabolic mirror will need the same amount of cooling in the three cases. In the aluminum case, the heating rate is two orders of magnitude less at the flat mirror than at the parabolic one, and in the Boral cases it is three orders of magnitude less. Thus the flat mirror may not need cooling at all, except as required for the laser light absorption at its surface, and any gamma heating, which remains to be estimated.

In the case of Boral as a duct liner, the heating rates are an order of magnitude higher than in the aluminum case, and may require separate cooling, especially for the reactor cavity liner which has a heating rate of about 1.4 Watts/cm^3, which is about the same as at the parabolic mirror face. Thus the reduction in neutron leakage by the use of Boral is achieved at the expense of a heating problem in the case of the Boral liner.

The heating rates in the lead mortar are slightly higher than in ordinary concrete. Both may require cooling depending upon their thermal conductivity.

The dose rates using the flux-to-dose rate factors given by Courtney [34] are also shown in Table X. At the quartz window a neutron dose rate of 1.2×10^6 rem/hr is obtained. One would like to reduce it to 100 mrem/hr outside the duct wall inside the reactor building. This extra seven orders of magnitude reduction could be achieved by the suggestions outlined in Section VI and needs further investigation.

III.3 Radiation Damage:

Table XI shows the calculated atomic displacement and gas production rates in different reactor components.

The dpa and gas productions at the parabolic mirror face are lower than previous estimates by Ragheb and Maynard [10], by about the $1/\cos\theta$ factor caused by the mirror tilt by an angle $\theta = 45°$. The dpa, He gas production, and H gas production were estimated earlier for a plain aluminum mirror front (here it is homogenized with water) as:

1.1710-07 $[\frac{dpa}{sec}]$, 5.3513-06 $[\frac{appm}{sec}]$, and 4.7199-06 $[\frac{appm}{sec}]$.

For Case III, they are:

6.9758-08 $[\frac{dpa}{sec}]$, 3.4861-06 $[\frac{appm}{sec}]$, and 3.0973-06 $[\frac{appm}{sec}]$.

The radiation damage at the flat mirror seems to be minimal compared to the parabolic mirror, thus it may not need replacement over a long period of time.

However, the radiation damage to the lead acetate tank wall is higher than the mirror itself. This is also true in other regions of the Boral lining, especially in terms of Helium production. It is another price we pay for reducing the neutron leakage by using Boral instead of Aluminum as a liner. The first price was the extra heating of the Boral. The reactor cavity liner will particularly suffer a high degree of radiation damage and will need frequent replacement.

The levels of hydrogen and helium gas production in the lead mortar are shown, and it remains to be studied with respect to dimensional changes. Previous shielding studies on concretes have not considered this problem since they were concerned with fission spectra, or fusion spectra for weapons shielding which are of short duration. Concretes are cheap and need to be investigated theoretically and experimentally for potential applications in laser-driven ICTR shielding. The potential application here is larger than in magnetic confinement work, since in the latter, space problems require optimum thickness shields between the blanket and toroidal field magnets, but here space is not constrained so that the shielding must be optimized with respect to cost and not to thickness.

We draw attention to our computation costs, as shown in Table XII. The low cost related to our exposed methodology in modelling the problem allows parametric scoping studies to be carried out by Monte Carlo, even for three-dimensional problems, at quite an economical expenditure.

III.4 Materials Activation and Afterheat:

Activation and afterheat analyses were carried out using the DKR fusion reactor radioactivity calculation code [42] and its associated data library DCDLIB [43]. The materials used included those from Table V for the case of Boral as liner and Lead Mortar as shield material. To allow for the effect of alloy composition of the aluminum, a composition was chosen that included 1.0 w/o chromium, 0.7 w/o iron, and 0.3 w/o copper along with the aluminum, corresponding to the alloy Al-6061 [16]. Analysis was also done to include a 1 mm layer of copper on the last mirror front surface, as suggested by Reichelt et al. [17]. The operating time of the reactor was taken as one year .

The activation of the last mirror is shown in Figure 9. The specific activity of the front surface, as well as the copper layer, is very high but when a smear activity is taken by weighting the activity by the volume, the effect is lessened. This comes about because the volumes of the copper layer (9.05×10^3 cm^3) and the front region (2.229×10^5 cm^3) are both small compared to the

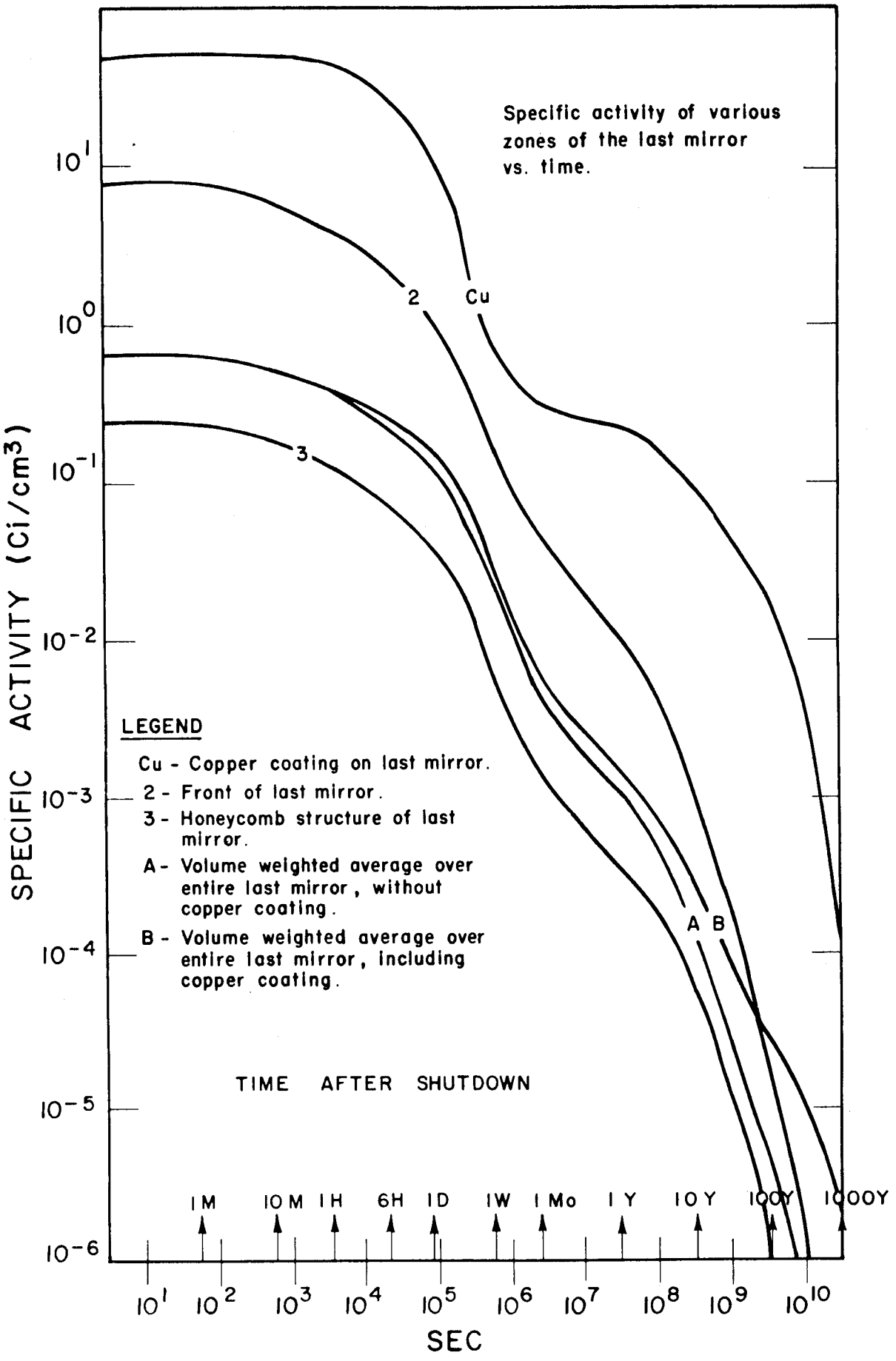
Specific activity of various zones of the last mirror vs. time.
SPECIFIC ACTIVITY (Ci/cm³)
10¹
10⁰
10⁻¹
10⁻²
10⁻³
10⁻⁴
10⁻⁵
10⁻⁶
Cu
2
3
A
B
LEGEND
Cu - Copper coating on last mirror.
2 - Front of last mirror.
3 - Honeycomb structure of last mirror.
A - Volume weighted average over entire last mirror, without copper coating.
B - Volume weighted average over entire last mirror, including copper coating.
TIME AFTER SHUTDOWN
1M
10M
1H
6H
1D
1W
1Mo
1Y
10Y
100Y
1000Y
10¹
10²
10³
10⁴
10⁵
10⁶
10⁷
10⁸
10⁹
10¹⁰
SEC

Figure 9

volume of the honeycomb structure (5.288×10^6 cm^3). It can be seen that the effect of adding the small copper layer is limited up until about 100 years after irradiation. The mirrors and surrounding structure activation may need remote handling for adjustment and maintenance.

The activation of the boral wall to the lead acetate tank exhibits roughly the same specific activation as the aluminum front surface of the last mirror. Figure 10 also shows the resultant activation of various other sections of the beam port liner. Activation to the same order of magnitude as the tank wall is seen in the reactor penetration lining. The activity of the other liner regions down the port then is an order of magnitude or more less than this value down to a reduction of four orders of magnitude at the flat mirror to quartz window lining.

The specific afterheat, shown in Figure 11, also follows this same general trend. Approximately the same afterheat is found in the lead acetate tank wall as the last mirror front surface. At shutdown this level (1.6×10^{-1} watts/cm^3) may need moderate cooling, and is retained up until about a week, but after this time, say at a month, maintenance and maybe machining could perhaps be performed directly on the mirror surface without cooling. At this time the specific afterheat would have dropped off over three orders of magnitude. Out in the lining

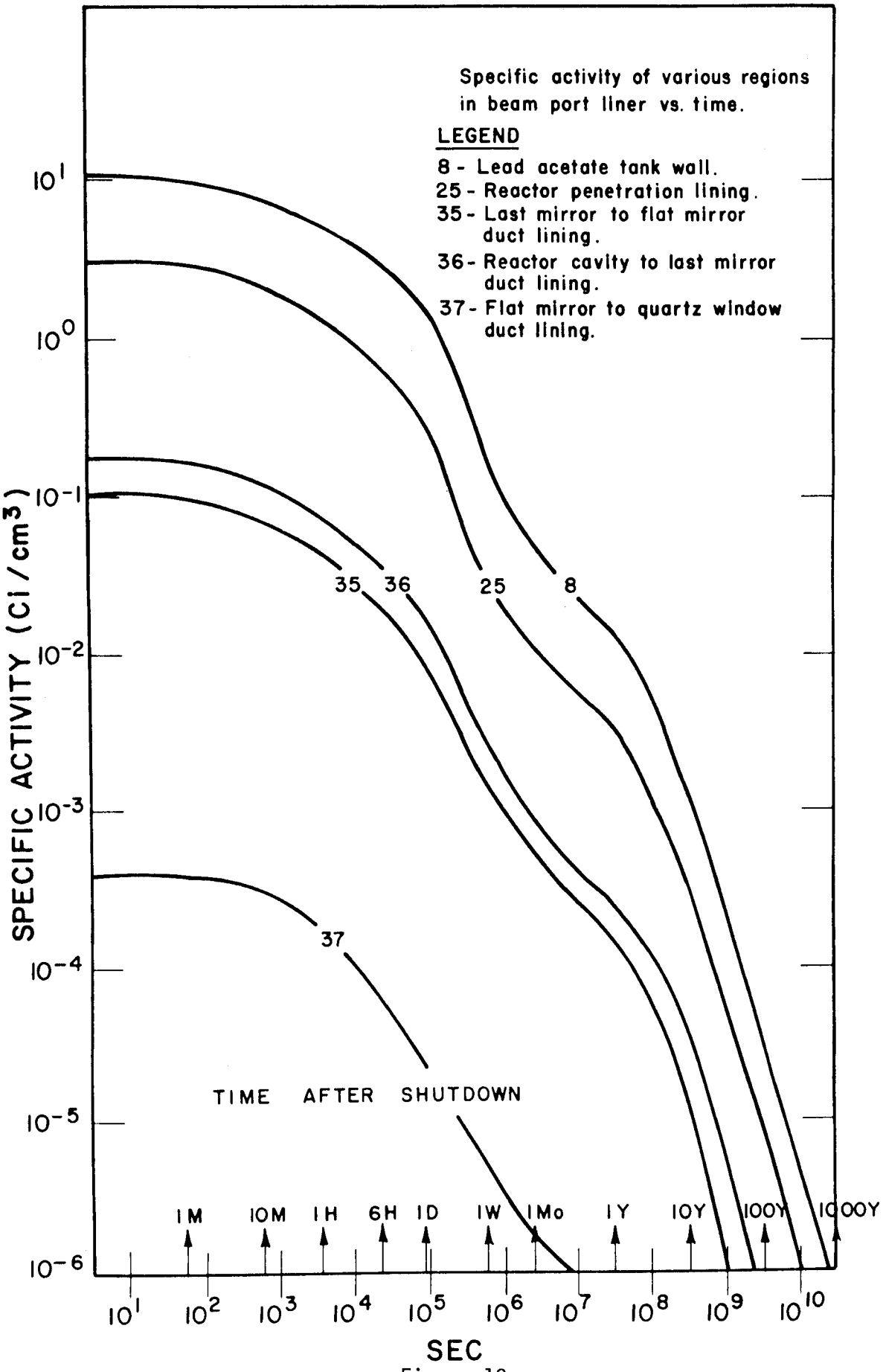
Specific activity of various regions in beam port liner vs. time.
LEGEND
8 - Lead acetate tank wall.
25 - Reactor penetration lining.
35 - Last mirror to flat mirror duct lining.
36 - Reactor cavity to last mirror duct lining.
37 - Flat mirror to quartz window duct lining.
SPECIFIC ACTIVITY (Ci/cm³)
10¹
10⁰
10⁻¹
10⁻²
10⁻³
10⁻⁴
10⁻⁵
10⁻⁶
35
36
25
8
37
TIME AFTER SHUTDOWN
1M
10M
1H
6H
1D
1W
1Mo
1Y
10Y
100Y
1000Y
10¹
10²
10³
10⁴
10⁵
10⁶
10⁷
10⁸
10⁹
10¹⁰
SEC

Figure 10

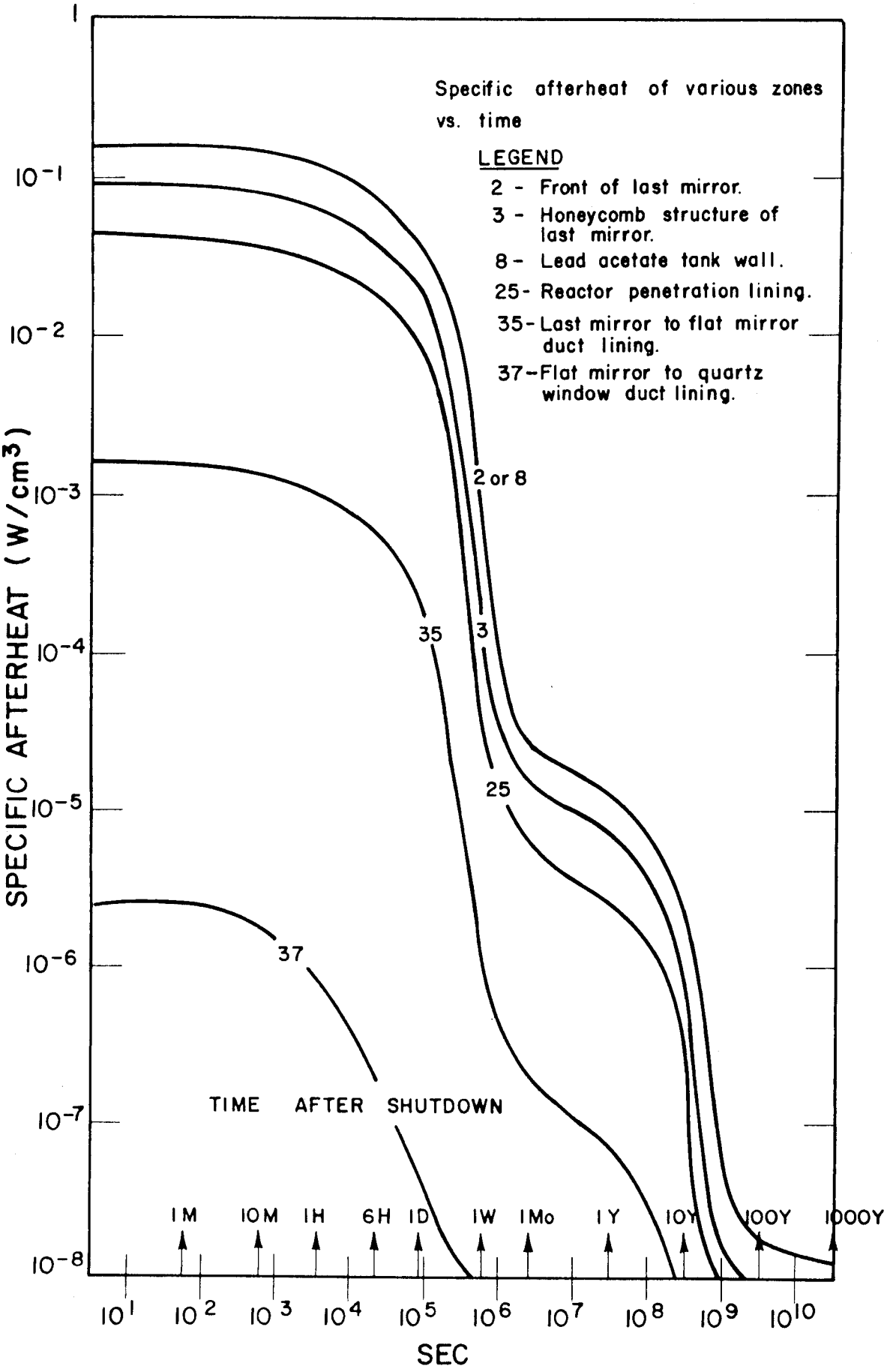
Specific afterheat of various zones vs. time
LEGEND
2 - Front of last mirror.
3 - Honeycomb structure of last mirror.
8 - Lead acetate tank wall.
25 - Reactor penetration lining.
35 - Last mirror to flat mirror duct lining.
37 - Flat mirror to quartz window duct lining.
2 or 8
3
25
35
37
SPECIFIC AFTERHEAT (W/cm3)
1
10-1
10-2
10-3
10-4
10-5
10-6
10-7
10-8
TIME AFTER SHUTDOWN
1M
10M
1H
6H
1D
1W
1Mo
1Y
10Y
100Y
1000Y
10 1
10 2
10 3
10 4
10 5
10 6
10 7
10 8
10 9
10 10
SEC

Figure 11

between the flat mirror and the quartz windows the specific afterheat never reaches a significant level.

At very short (0 to 1 day) post-irradiation times the major contributing isotopes to the specific activity in the last mirror are ^{24}Na and ^{27}Mg from the aluminum and ^{64}Cu in the copper layer. The impurities in the aluminum alloy 6061 do not appreciably affect the results in this time frame. However, after about one month to one hundred years ^{55}Fe and ^{63}Ni dominate the radioactivity. Therefore, if high purity aluminum could be used rather than Aluminum alloys, the activity level during this time span would be appreciably reduced. At very long post-irradiation times the major portion of the activation once again is due to aluminum, specifically ^{26}Al.

IV. LIMITATIONS OF THE MODEL:

In the Monte Carlo calculations, it was assumed that the source particles originate in the first neutron group which has a midpoint energy of 14.208 Mev. However, each D-T reaction produces a 3.52 Mev α-particle with its energy deposited locally within the pellet and one 14.1 Mev neutron (a total of 17.62 Mev). This neutron deposits some of its energy in the pellet and produces secondary gamma rays. Radiation from the pellet consists of a 14.1 Mev neutron component, a lower-energy degraded neutron component, and secondary γ-rays. Thus adequate computations should consider in the future both the neutron and gamma spectra of the source. These can be inferred from the corresponding pellet neutronics studies.

We suggest adjusting the first neutron group limits so that its midpoint is 14.1 Mev. The α particle energy deposition has not been considered in our study, but will be deposited in the carbon liner and at the mirror front and contributes to the overall heating. The same applies to the pellet x-rays.

In the estimation of heating rates and neutron primary damage parameters (dpa, gas production), a laser fusion event is considered to release a power of 3×10^3 MW, equivalent to:

$$S = 3 \times 10^3 \text{ (MW)} \times 10^6 \text{ (W)} \times \frac{1}{1.6021 \times 10^{-13}} \text{ (sec)} \times \frac{1}{17.62}$$

$$= 1.063 \times 10^{21} \left(\frac{\text{source neutrons}}{\text{sec}}\right)$$

However, assuming pellet losses to be 0.11 MeV, an example of a pellet output can be written as [18] :

α-particle energy deposition in pellet	3.52 Mev
Neutron escape from pellet	12.20 Mev
Nuclear energy absorbed in pellet	0.89 Mev
γ-ray leakage from pellet	0.90 Mev
Total energy per D-T reaction in the pellet	17.51 Mev

which changes the normalization to: $S' = S \cdot \frac{17.62}{17.51} = 1.069 \times 10^{21}$ $(\frac{\text{source neutrons}}{\text{sec}})$. This will affect the estimated parameters of interest, especially tritium breeding, leakage flux and damage parameters. Also, the final neutron heating rate estimates should be adjusted by multiplying the point-source values by: (12.2/14.208) = 0.859. This normalization may be adequate for direct neutron heating rates, but not for leakage estimates and for tritium production in the blanket from Li^6. If a low energy neutron component escapes from the pellet after suffering energy degradation, a correction is necessary. The number of endoergic breeding reactions with Li^7, which interacts with high energy neutrons, decreases, whereas the number of exoergic breeding reactions with Li^6, which interacts with slow neutrons, increases. Neutron multiplication in the pellet also occurs via (n,2n) reactions. These effects can be corrected only by coupled pellet-blanket-shield neutronics and photonics calculations. Due to the preliminary nature of our studies, these effects were not considered.

The results obtained are time-integrated over a laser pulse duration. Time-dependent values may be obtained by the Monte Carlo calculations. The source time-dependence can be taken into account. A larger number of particle histories would be necessary for such studies.

V. CONCLUSIONS AND SUGGESTIONS FOR FURTHER INVESTIGATIONS

In this work, we employed a three-dimensional economically attractive modeling of laser-driven reactor penetrations. The particle leakage was found excessively high for the configuration of the conceptual design considered. Use of Boral as a duct liner succeeded in reducing the radiation leakage by an order of magnitude, but raised a cooling requirement in some parts of the duct lining, and a radiation damage problem. Using lead mortar instead of ordinary concrete as a shield material does not reduce the leakage appreciably, even though it is potentially better as a shielding material, especially for the gamma rays. Thus the radiation leakage is identified as the main area of concern for such designs. Until now, it was thought that the main area of concern was the heating and radiation damage to the last mirror. The radiation damage and heating to parts of the laser beam duct are identified as comparable to similar problems in the cavity first wall. More importantly, it is established that material compositions alone cannot control the leakage problem, and that these choices must be supplemented by alternative geometrical configurations. The last aspect requires a close interaction between the shielding and beam transport engineering. Mirrors may need remote handling and afterheat cooling.

The following approaches require further investigation of their effectiveness in reducing the radiation leakage, both neutron and gamma:

1. A major cause of the observed leakage problem is simply that the ducts are too large. The penetration is 240 cm in diameter offering long paths for the leaking particles. Abdou [2] reports that in Tokamak reactors employing neutral beam injectors: "... the neutron flux at the TF coils is approximately proportional to d^4, where d is the characteristic dimension of the penetration cross section...". Thus one can suggest:
   a) Increasing the number of used beams. This will lead to a smaller characteristic dimension of the penetration and to a better uniformity in pellet illumination, but may jeopardize the system economics. If a circular beam is divided into n equivalent beams so that the beam cross sectional area is preserved, the surface area of the penetration is also increased by a factor of $\sqrt{n}$, leading to more absorption of the leaking radiation in the walls.
   b) Controlling the cross sectional shape of the laser beam. Elongated rectangles and annular beams will have a smaller characteristic dimension d, and subsequently decreased leakage; see Figure 12.d.
   c) Beam Cross-over. Use of cylindrical-parabolic mirrors allows a line cross-over, and use of spherical and paraboloid mirrors allows a point cross-over of the beam [41].

Around the cross-over region shielding can be provided with a minimal characteristic dimension for the penetration. The limitation here is the filling gas breakdown because of the high light intensity at the cross-over region. See Figures 12-a and 12-b.

2. Use of flux traps. This is a standard shielding technique where the surface area of the penetration seen by both the detector and source is minimized. Tapering and untapering of the penetration wall can be used, as shown in Figure 12-c. The particles in the flux traps scatter several times, lose their energy, and get absorbed in the penetration liner, rather than directly leaking through the duct.
3. Use of an extra mirror reflection. This leads to an extra segment in the duct, decreasing leakage.
4. Use of multiple reflection catotropic optics as suggested in Reference 18, after the flat mirror, is expected to appreciably reduce leakage.
5. Use of smaller turning angles. As shown in Table I, this leads to smaller size mirrors and subsequently smaller subtended solid angles by the last optical element.
6. Iris type rotating choppers can be used to mechanically close the duct at times when the laser beam pulse is

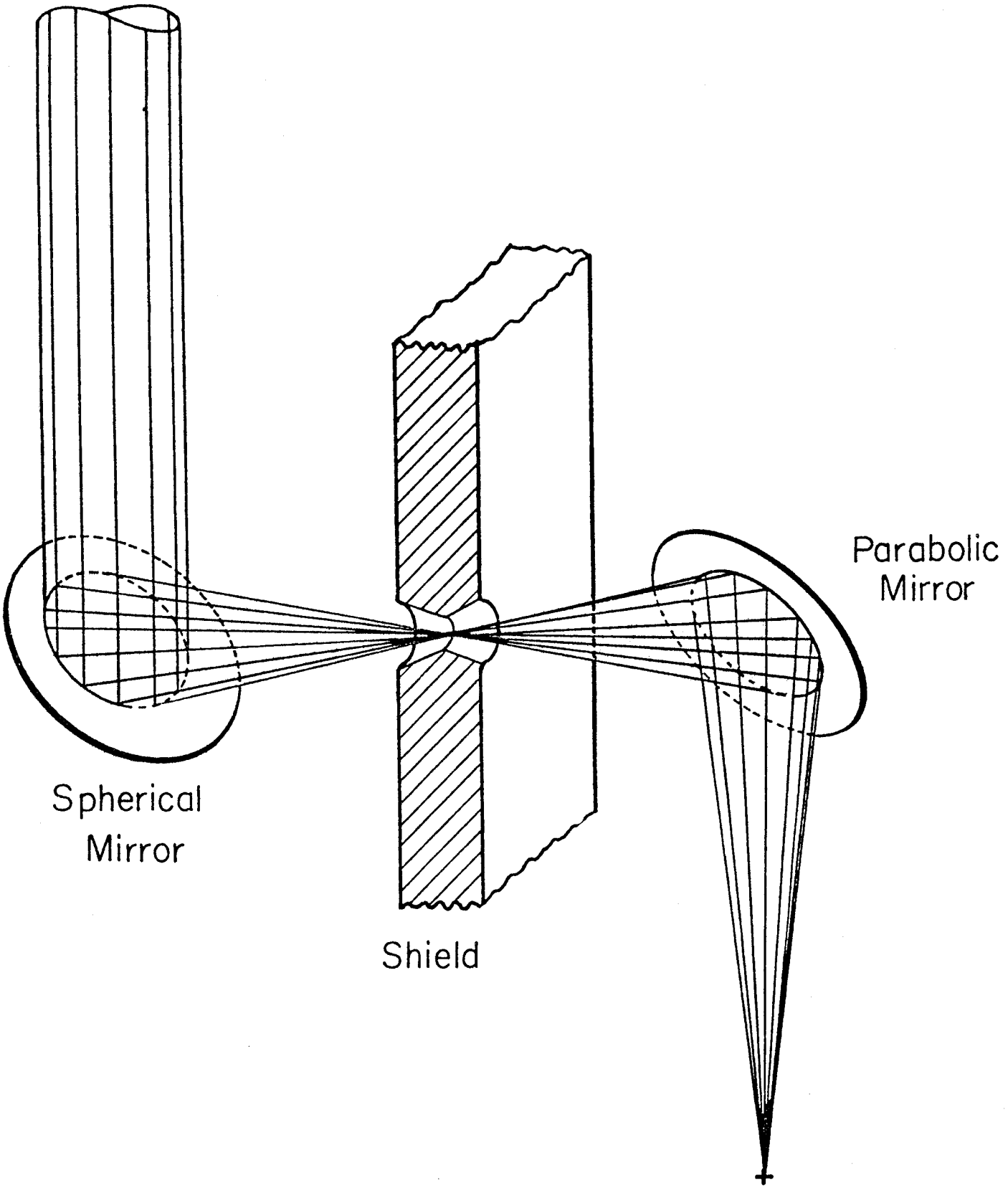

Point Cross-Over

Figure 12.a

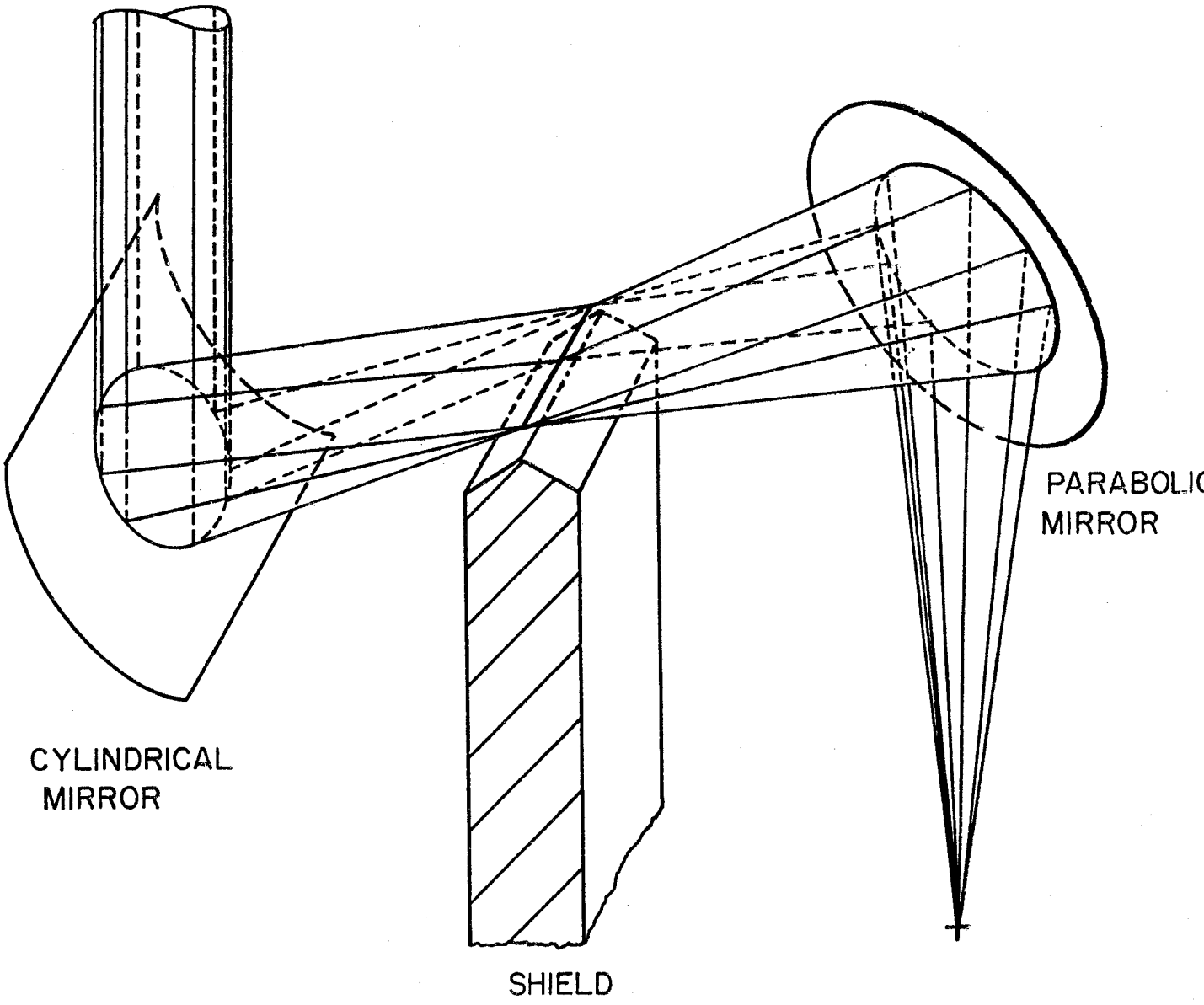

LINE CROSS-OVER

Figure 12.b

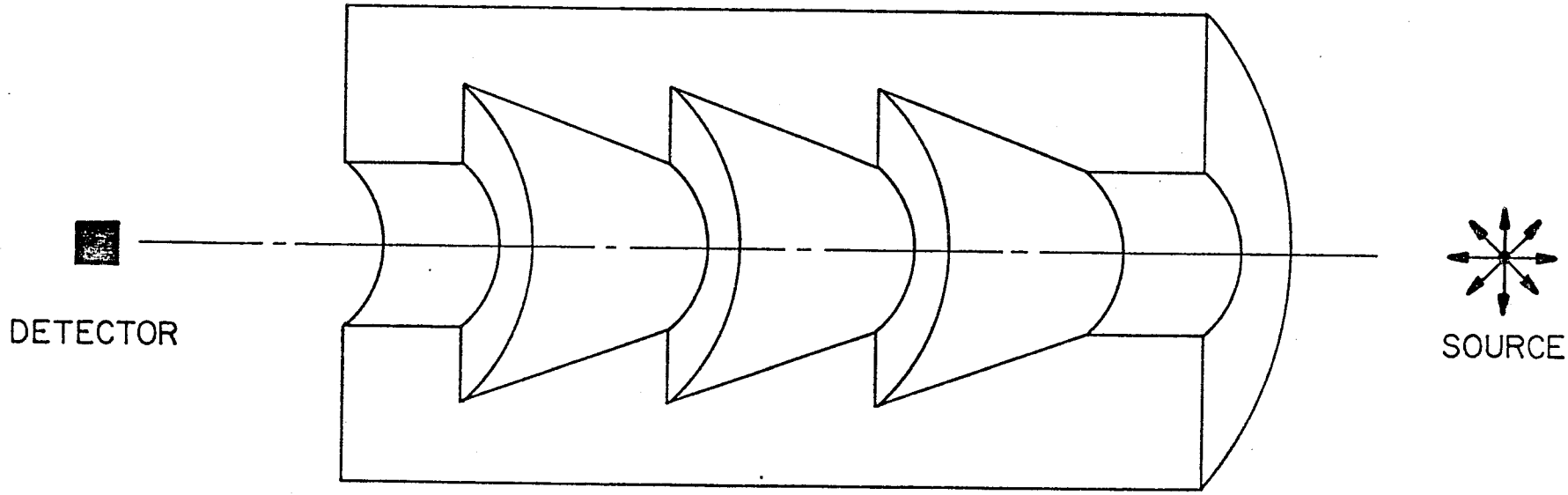

PENETRATION WITH FLUX TRAPS

Figure 12.c

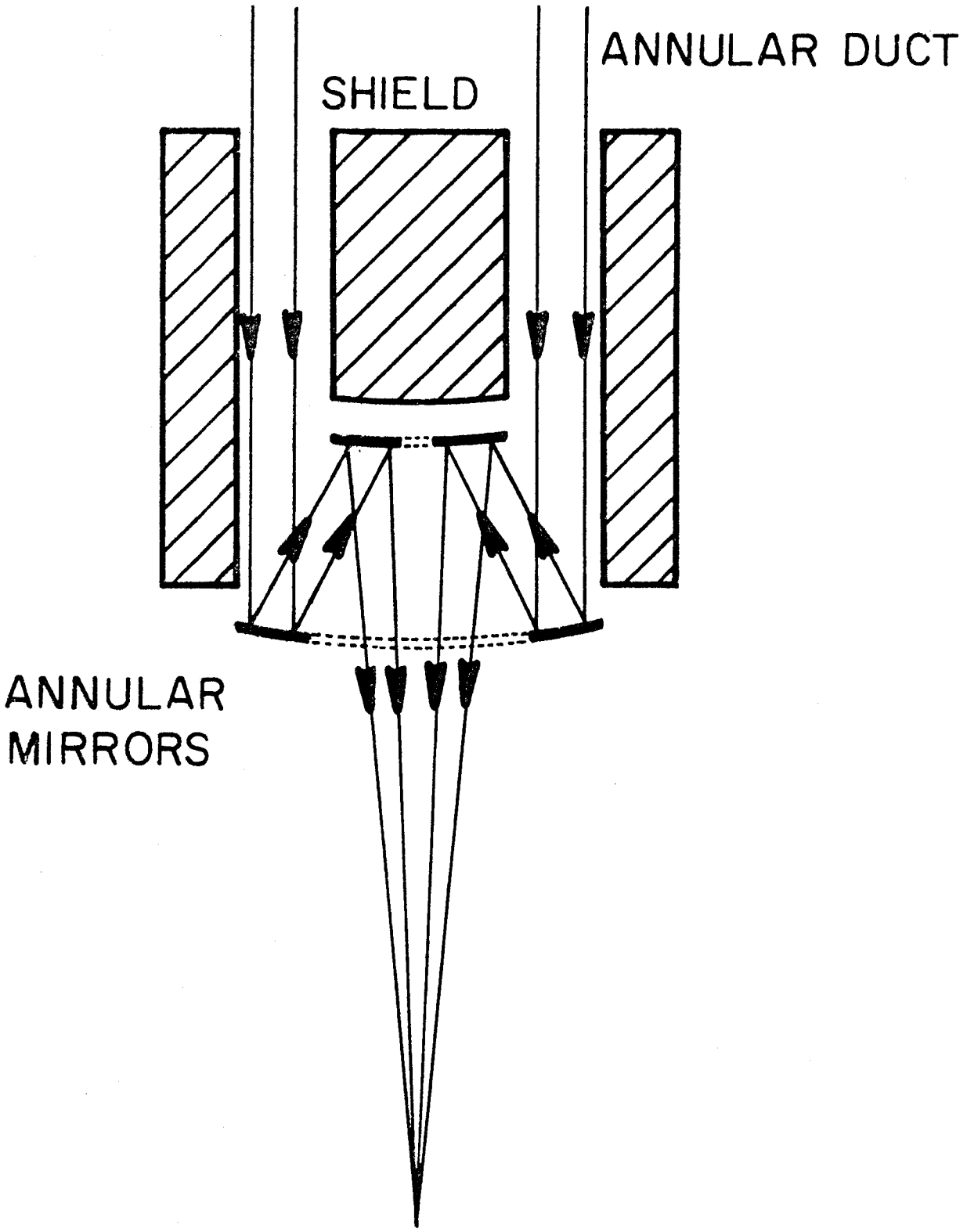

ANNULAR–BEAM ILLUMINATION

Figure 12.d

not travelling through it. This is only possible at low microexplosion repetition rates.

7. Locating the last mirror further from the cavity center (large f-number optics) is the most effective direct way of reducing the shield angle of the duct as shown in Table I. Recourse to this approach has limits, and must be a last resort since it increases the plant size and cost, and leads to problems regarding misalignment and outfocusing of the beams in a plant vibration environment.
8. Inspection of Figure 8 shows that the very low and high energy parts of the radiation spectrum have been essentially eliminated in Regions 7 and 8. The energy range from a few kev to a few Mev is still a major radiation source. The use of materials such as Tungsten and water that are particularly good moderators in key zones may substantially reduce the radiation in this energy range.
9. Use of gas refraction lenses which use supersonic gas streams to set up a density distribution forming a prism of higher index of refraction material which will bend light, but not neutrons or debris [46].

Our analysis and modelling of a laser reactor penetration identifies the radiation leakage problem as a major area of con-

cern, in addition to the radiation damage to the last mirror. As currently thought, it is the main consideration, especially if dielectric coatings of the mirror surface are necessary, and uncoated mirrors cannot be used [46]. A combination of the outlined suggestions will have to be adopted to reach acceptable design criteria for the radiation leakage in a viable laser-driven reactor system.

REFERENCES

1. Ide, T., Seki, Y. and Iida, H., "Effects of Neutron Streaming through Injection Ports on Neutronic Characteristics of a Fusion Reactor," Proc. of the Second Topical Meeting on the Technology of Controlled Nuclear Fusion, Vol. II, p. 395, Sept. 21-23, Richland, Washington, (1975).

2. Abdou, M.A, Milton, L.J., Jung, J.C. and Belbar, E.U., "Multidimensional Neutronic Analysis of Major Penetrations in Tokamaks," Proc. of the Second Topical Meeting on the Technology of Controlled Nuclear Fusion, Vol. II, p. 845, Sept. 21-23, Richland, Washington, (1975).

3. Santoro, R.T., Tang, J.S., Alsmiller, R.G., Jr., and Barnes, J.M., "Monte Carlo Analysis of the Effects of a Blanket-Shield Penetration on the Performance of a Tokamak Fusion Reactor," ORNL/TM-5874, May (1977).

4. Ragheb, M.M.H., Cheng, E.T., and Conn, R.W., "Monte Carlo and Discrete Ordinates Investigations for a Laser Reactor Li_2O Blanket," accepted for publication in Atomkernenergie (1978).

5. Ragheb, M.M.H., Cheng, E.T., and Conn, R.W., "Monte Carlo Study of Asymmetry Effects in a Magnetically-Protected-First-Wall Laser Driven Reactor," accepted for publication in Atomkernenergie (1978).

6. Cheng, E.T. Ragheb, M.M.H., and Conn, R.W., "Neutronics and Photonics Studies for the University of Wisconsin Laser Fusion Reactor Blanket," Trans. Am. Nucl. Soc., 26, p. 504 (1977).

7. Ragheb, M.M.H., Gohar, Y.M., and Maynard, C.W., "Effect of Particles Histories Termination Parameters on Monte Carlo Estimates in Fusion Reactor Blanket Scoping Studies," UWFDM-192, Univ. of Wisconsin (1977).

8. Ragheb, M.M.H. and Maynard, C.W., "Three-dimensional Cell Calculations for a Fusion Reactor Gas-Cooled Solid Blanket," UWFDM-92 Revised, Univ. of Wisconsin (1977).

9. Ragheb, M.M.H. and Maynard, C.W., "Effect of Experiment-size Parameters on Monte Carlo Estimates in Fusion Reactor Blanket Simulations," UWFDM-206, Univ. of Wisconsin (1977).

10. Ragheb, M.M.H and Maynard, C.W., "Calculated Neutron and Gamma Irradiation Response of Actively Cooled Mirrors for Laser Fusion Power Reactors", UWFDM-218, Univ. of Wisconsin (1978).

11. Hansen, L.F. and Maniscalco, J.A., "Neutronics Study of a Laser Fusion Hybrid Reactor Design," UCRL-78069, Sept. (1976).

12. Ragheb, M.M.H. and Maynard, C.W., " A Version of the MORSE Multigroup Transport Code for Fusion Reactor Blankets and Shield Studies," BNL-20376, Brookhaven National Laboratory (1975).

13. RSIC Code Package CCC-203, "MORSE-CG," Radiation Shielding Information Center, ORNL (1976).

14. Emmett, M.B., "The MORSE Monte Carlo Radiation Transport Code System," ORNL-4972, Oak Ridge National Laboratory (1975).

15. Howard, J., "Imaging Properties of Off-axis Parabolic Mirrors," UWFDM-214, Univ. of Wisconsin (1977).

16. Stark, E., "Laser Fusion Program," LA-6510-PR, Los Alamos Scientific Laboratory (1976).

17. Reichelt, W.H., Belvins, D.J., and Turner, W.D., "Metal Optics in CO_2 Laser Fusion Systems," La-UR-77-468, Los Alamos Scientific Laboratory (1977).

18. Booth, L.A., "Central Station Power Generation by Laser-Driven Fusion," LA-4858-MS, Vol. 1, Feb (1972).

19. Gohar, Y.M. and Maynard, C.W., Personal Communication.

20. Conn, R.W., Abdel-Khalik, S., Moses, G.A., Cheng, E.T., Cooper, G., Howard, J., Kulcinski, G.L., Larsen, E., Lovell, E., Magelssen, G., Sviatoslavsky, I., Wolfer, W., Beranek, F., Chang, S.K., Droll, R., Ghoniem, N., Hunter, T., Ortman, M., Spencer, R., Shuy, G. and Ragheb, M.M.H., "Studies of the Technological Problems of Laser Driven Fusion Reactors," UWFDM-190, Univ. of Wisconsin (1976).

21. Conn, R.W., Abdel-Khalik, S.I., Moses, G.A., Beranek, F., Cheng, E.T., Cooper, G.W., Droll, R.B., Henderson, T., Howard, J., Hunter, T.O., Larsen, E.M., Kulcinski, G.L., Lovell, E.G., Magelssen, G.R., Maynard, C.W., Ortman, M., Ragheb, M.M.H., Rensel, W.B., Solomon, D., Spencer, R.L., Sviatoslavsky, I.N., Vogelsang, W.F., Watson, R.D., and Wolfer, W.G., "SOLASE, A Conceptual Laser Fusion Reactor Design," UWFDM-220, Univ. of Wisconsin (1978).

22. Jaeger, T.A., Eisenlohr, H.H., Editors, "Engineering Compendium on Radiation Shielding," Volume II, Shielding Materials, IAEA, Springer-Verlag, (1975).

23. Rockwell III, T., Editor, "Reactor Shielding Manual," D. Van Nostrand Company, Inc., (1956).

24. Trubey, D.K. and Emmett, M.B., "Some Calculations of the Fast-Neutron Distribution in Ordinary Concrete from Point and Plane Isotropic Fission Sources," ORNL-RSIC-4, Oak Ridge National Laboratory, (1965).

25. 13.8/Ch, "Metallic Mortars by Chemtree Corporation," Chemtree Park, Central Valley, New York (1977). Communicated by Mr. Wm. Cornelius Hall, President and Chief Scientist.

26. Weast, R.C., Editor, "CRC Handbook of Chemistry and Physics," 54-th Edition, CRC Press (1973).

27. DLC-37B Data Library, Radiation Shielding Information Center, Oak Ridge National Laboratory, (1975).

28. Plaster, D.M., Santoro, R.T., and Ford, W.E., III, "Coupled 100-group Neutron and 21-Group Gamma Ray Cross Sections for EPR Calculations," ORNL-TM-4872, Oak Ridge National Laboratory, (1975).

29. Ford, W.E., III, Santoro, R.T., Roussin, R.W., and Plaster, D.M., "Modification Number One to the Coupled 100n-21 γ Cross Section Library for EPR Calculations," ORNL-TM-4259, Oak Ridge National Laboratory, (1976).

30. Abdou, M.A. and Roussin, R.W., "MACKLIB, 100 Group Neutron Fluence-to-Kerma Factors and Reaction Cross Sections Generated by the MACK Computer Program from Data in ENDF Format," ORNL-TM-3995, (1974).

31. Avci, H., and Kulcinski, G.L., "The Response of ISSEC Protected First Walls to DT and DD Plasma Neutrons," UWFDM-135, The Univ. of Wisconsin, (1975).

32. Gabriel, T.A., Auburget, J.D., and Greene, N.M., "Radiation Damage Calculations: Primary Recoil Spectra, Displacement Rates, and Gas Production Rates," ORNL-TM-5160, Oak Ridge National Laboratory, (1976).

33. Joanou, G.D., and Dudek, J.S., "GAMII A B3 Code for the Calculation of Fast Neutron Spectra and Associated Multigroup Constants," GA-4265, General Atomic, (1973).

34. Courtney, J.C., Editor, "A Handbook of Radiation shielding Data," Nuclear Science Center, Louisiana State University, and Shielding and Dosimetry Division, ANS, April (1975).

35. Lovell, E., Personal Communication, Fusion Technology Program, The Univ. of Wisconsin.

36. Maniscalco, J.A., Meier, W.R., and Monsler, J.J., "Conceptual Design of a Laser Fusion Power Plant," Trans. Am. Nucl. Soc., 27, 34 (1977).

37. Conn, R.W., Abdel-Khalik, S.I., and Moses, G.A., "SOLASE, A Laser Fusion Reactor Study," Trans. Am. Nucl. Soc., 27, 36 (1977).

38. Abdel-Khalik, S.I., Conn, R.W., Moses, G.A., Cheng, E.T., Larsen, E.M., Lovell, E.G., Maynard, C.W., Sviatoslavsky, I.N., and Wolfer, W.G., "Engineering Design Aspects for SOLASE," Trans. Am. Nucl. Soc., 27, 37, (1977).

39. Moses, G.A., Conn, R.W., Abdel-Khalik, S.I., Cooper, G.W., Howard, J.E. and Magelssen, G.R., "Laser Optics and Pellet Design for SOLASE," Trans. Am. Nucl. Soc., 27, 38 (1977).

40. Cooper, G.W., "Laser Design Considerations for an Inertially Confined Fusion Reactor," Trans. Am. Nucl. Soc., 27, 35, (1977).

41. Howard, J., "Personal Communication."

42. Sung, T.Y. and Vogelsang, W.F., "DKR: A Radioactivity Calculation Code for Fusion Reactors", UWFDM-170, Univ. of Wisconsin, (1976).

43. Sung, T.Y. and Vogelsang, W.F., "Decay Chain Data Library for Radioactivity Calculations", UWFDM-171, Univ. of Wisconsin, (1976).

44. Sletten, C.J., "Reflector Antennas", in: Collin, E.J., and Zucker, F.J., "Antenna Theory", Part 2, Inter-University Electronics Series, Vol. 7, McGraw-Hill, p. 37 (1969).

45. Strange, B.J., and Rice, B.J., "Analytic Geometry and Calculus with Technical Applications", John Wiley and Sons, p. 275, (1970).

46. Monsler, M.J. and Maniscalco, J.A., "Optical Design Considerations for Laser Fusion Reactors", UCRL-79990, Lawrence Livermore Laboratory (1977).

APPENDIX

The concave surface of the paraboloidal reflector, or ubiquitous "dish", is the most frequently used reflector antenna [44], and solar concentrator. Off-axis paraboloid mirrors have been suggested for simultaneously turning and focusing collimated laser beams. In a geometrical optic sense a mirror of this form focuses an incident electromagnetic plane wave propagating parallel to its axis to the focal point of the paraboloid of revolution and is considered "unaberrated" [44]. We shall outline some of the geometrical relationships for such a mirror with focal length, "a", its focal line coincident with the z-axis, and the focal point lying at the origin of the coordinate system as shown in Figure A.1.

In the plane z-y, as shown in Figure A.2, we have:

$$GP = OP \tag{A.1}$$

according to the definition of the parabola as the set of all points equidistant from a fixed point (focus) and a fixed line (directrix) [45]. From Figure A.2:

$$GP = 2a - z$$

$$OP = \sqrt{z^2 + y^2}$$

Substituting in Equation A.1 and squaring both sides, expanding and collecting terms, the equation of the parabola in the y-z plane becomes:

$$y^2 = 4a(a - z) \tag{A.2}$$

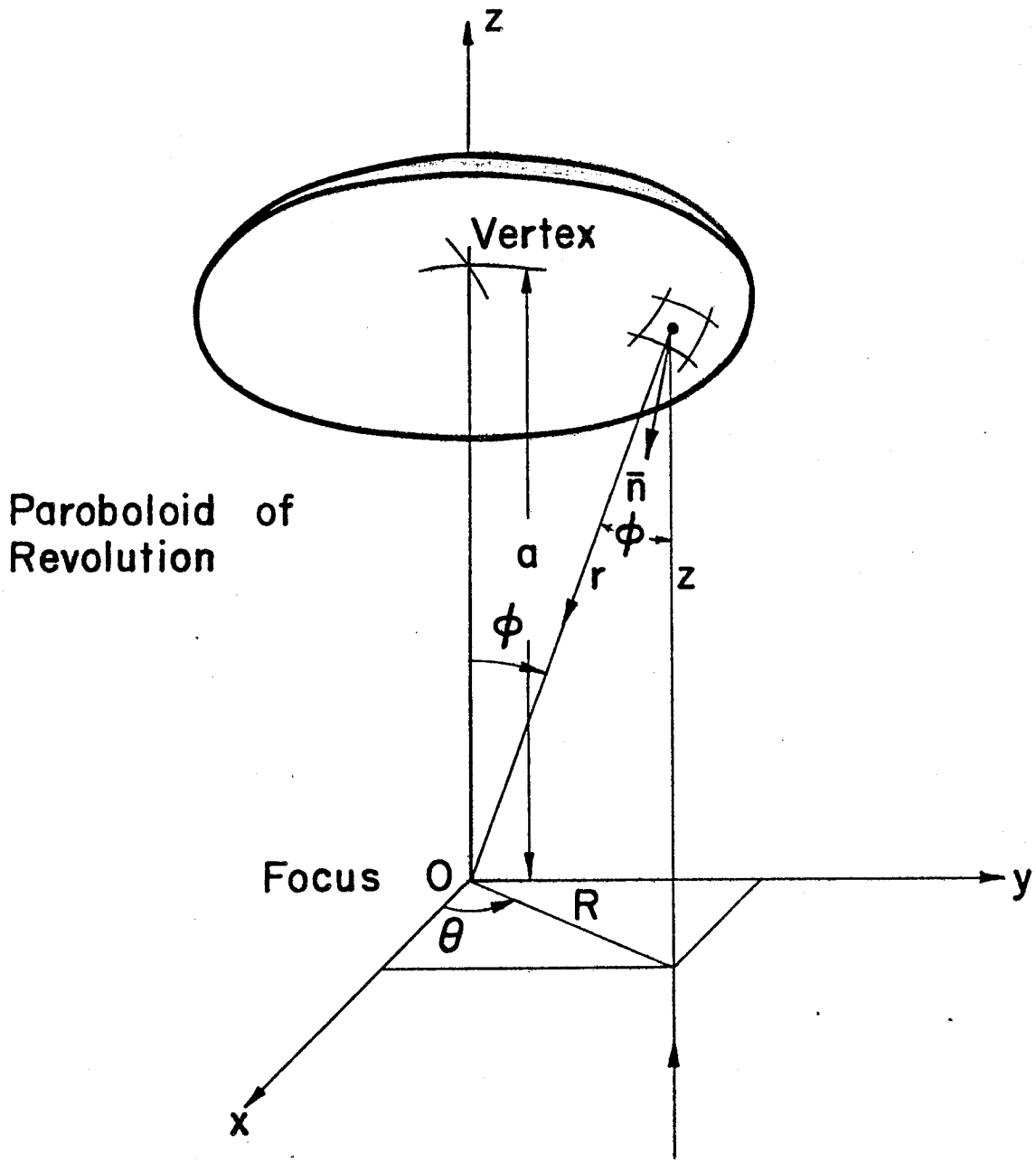
z
Vertex
Paraboloid of Revolution
a
r
$\bar{n}$
ϕ
z
ϕ
Focus O
R
θ
y
x

Figure A.1

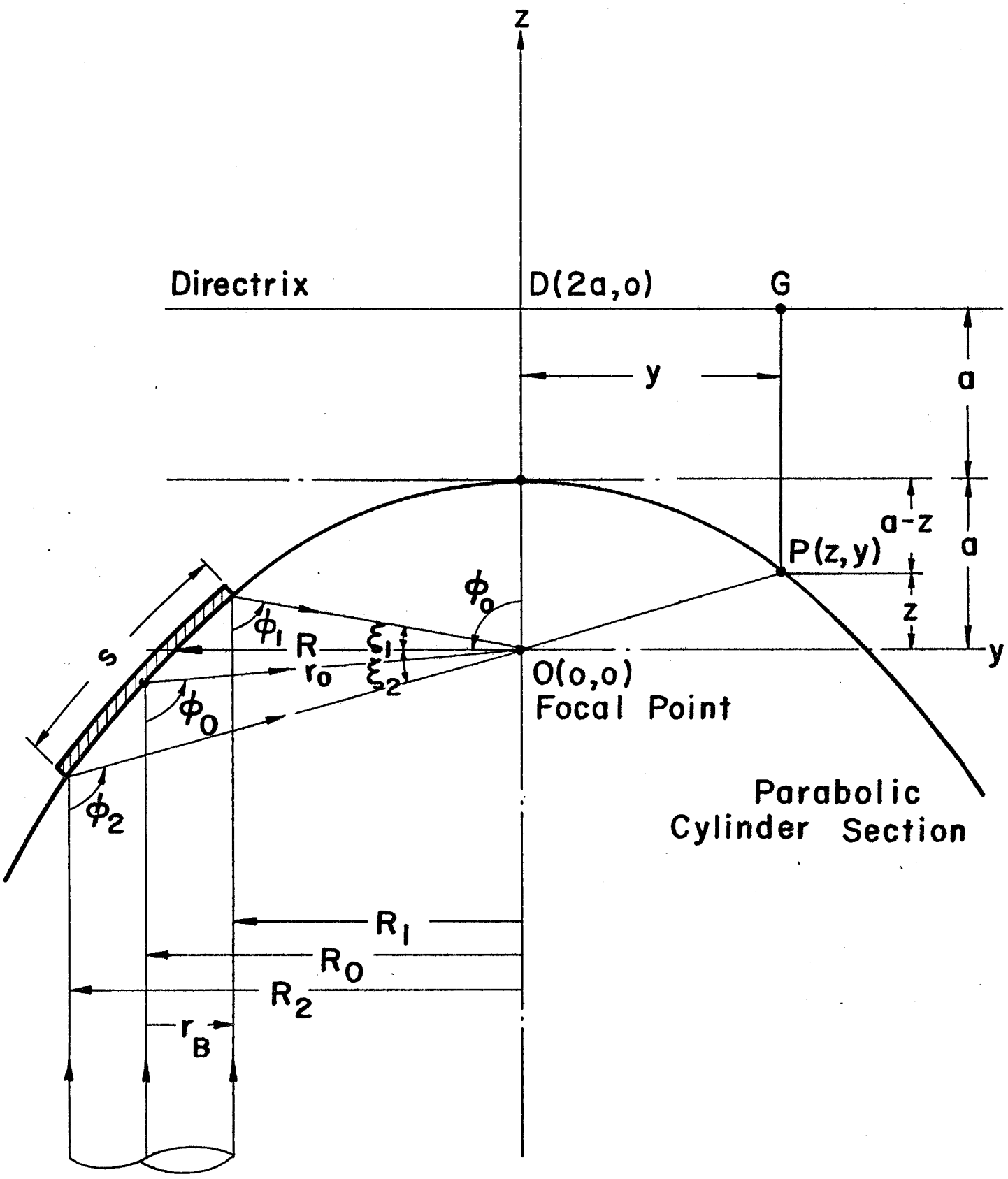
Z
Directrix
D(2a,o)
G
y
a
a-z
P(z,y)
a
z
y
ϕ_0
ϕ_1
R
ξ_1
s
r_0
ξ_2
O(o,o)
Focal Point
ϕ_0
ϕ_2
Parabolic
Cylinder Section
R_1
R_0
R_2
r_B

Figure A.2

Equation A.2 can be generalized to the case of the paraboloid of revolution of Figure A.1 by replacing y^2 by $R^2 = x^2 + y^2$, which leads to:

$$R^2 = x^2 + y^2 = 4a(a - z) \qquad (A.2)'$$

in cylindrical (R,z,θ) and cartesian (x,y,z) coordinates.

Equation (A.2)' can be converted to spherical (r,ϕ,θ) coordinates by substituting for x, y, z in (A.2)' and solving for a quadratic in r as:

$$r = \frac{2a}{1 + \cos\phi} \qquad (A.3)$$

From Equation A.3 and Figure A.1:

$$R = r\sin\phi = \frac{2a\sin\phi}{1 + \cos\phi} \qquad (A.4)$$

Substituting for $\cos\phi = \sqrt{1 - \sin^2\phi}$ in the last equation, isolating the square root on one side, then squaring both sides, we get:

$$\phi = \sin^{-1}\frac{4aR}{4a^2 + R^2} \qquad (A.5)$$

From which:

$$\phi_1 = \sin^{-1}\frac{4aR_1}{4a^2 + R_1^2}, \quad \phi_2 = \sin^{-1}\frac{4aR_2}{4a^2 + R_2^2} \qquad (A.6)$$

where $R_1 = R_o - r_B$

$R_2 = R_o + r_B$

R_o is the distance between the beam and paraboloid axes

r_b is the beam radius

From the geometry:

$$\xi_1 = \phi_o - \phi_1$$
$$\xi_2 = \phi_2 - \phi_o \qquad (A.7)$$

where ϕ_o can be obtained from Equation A.5 by substituting R = R_o.

The solid angle subtended by the conical section of half angle ξ will be:

$$\Omega = \frac{\int dA}{r^2} = \frac{\int_0^{\xi}\int_0^{2\pi} r^2 \sin\phi \, d\theta \, d\phi}{r^2}$$
$$= 2\pi(1 - \cos\xi) \qquad (A.8)$$

The radius of curvature of the mirror can be calculated from [15]:

$$R_c = 2a \sec^3\left(\frac{\phi}{2}\right) \qquad (A.9)$$

and the arc length of the mirror along the longer dimension of the approximately elliptical spot projected by the cylindrical beam on the mirror is [15]:

$$s = \int_{R_1}^{R_2} \sqrt{1 + \left(\frac{dz}{dR}\right)^2}\, dR = 2a \int_{u_1}^{u_2} \sqrt{1 + u^2}\, du$$
$$= a\left[u_2\sqrt{1 + u_2^2} - u_1\sqrt{1 + u_1^2} + \ell n\left[\frac{u_2 + \sqrt{1 + u_2^2}}{u_1 + \sqrt{1 + u_1^2}}\right]\right]$$

where: $u_1 = \frac{R_1}{2a}$, $u_2 = \frac{R_2}{2a}$ (A.10)

The relationships A.1 to A.10 can be used to compute the characteristics of paraboloid of revolution laser mirrors.

Table I

Comparison of Parabolic Mirrors With Different Parameters

	Case A	Case B	Case C	Case D
Laser Beam Radius, r_B(m)	1.000	1.00	1.000	1.000
Position from Cavity Center, r_o(m)	10.000	15.00	20.000	15.000
Latus rectum of Parabola, a(m)	5.000	7.500	10.000	8.800
Turning Angle, ϕ_o	90°	90°	90°	80°
R_o(m)	10.000	15.000	20.00	14.770
Mirror Largest Dimension,				
s(m)	2.830	2.828	2.829	2.611
1.2 s(m)	3.396	3.394	3.394	3.133
Radius of Curvature R_c(m)	28.280	42.430	56.568	39.162
ϕ_1	83.97°	86.05°	87.06°	76.07°
ϕ_2	95.45°	93.70°	92.80°	83.71°
ξ_1	6.03°	3.95°	2.94"	3.92°
ξ_2	5.45°	3.70°	2.80°	3.71°
Subtended Solid Angle (steradian)	0.035	0.015	0.008	0.015

For Case A:

ϕ_o	30°	45°	60°	75°	90°	105°	120°	135°
s(m)	2.08	2.15	2.30	2.50	2.83	3.25	4.00	5.23

Table II

Elemental Compositions of Materials Mixes

	Material Mixes	Elements	Atomic Densities atoms/(barn·cm)
1	Mirrors Fronts and Rear Sides 25 v/o H_2O + 75 v/o Al $\rho(H_2O)$ = 1.0 (gm/cm^3), ρ(Al) = 2.699 (gm/cm^3)	Al-27 H† O-16	0.045183 0.016715 0.008358
2	Mirrors Honeycomb Structure ρ(Al) = 0.083304 (gm/cm^3)	Al-27	0.001859
3	Linings for Shields and Beam Port		
	I - Aluminum, ρ(Al) = 2.699 (gm/cm^3)	Al-27	0.060244
	II - Boral: 36.5912 v/o B_4C + 63.4088 v/o Al ρ(Boral) = 2.143180 (gm/cm^3) ρ(Al) = 2.699 (gm/cm^3) $\rho(B_4C)$ = 1.18 (gm/cm^3) w/o B_4C = 20.1465, w/o Al = 79.8535 N(B-10)/N(B-11) = 0.246875	Al-27 C-12 B-10 B-11	0.038200 0.004706 0.003690 0.015134
4	Lead Acetate Solution + Boral Shield 95 v/o $Pb(C_2H_3O_2)_2$ Solution + 5 v/o Boral $Pb(C_2H_3O_2)_2$ Solution is: 35.0649 v/o $Pb(C_2H_3O_2)_2$ + 64.9351 v/o H_2O	Pb H O-16 B-10 B-11 C-12 Al-27	0.002527 0.056409 0.030732 0.000185 0.000757 0.010344 0.001910
5	Ordinary Concrete or Lead Mortar Shield		
	I - Ordinary concrete ρ = 2.3 (gm/cm^3) 24.33 w/o Ca + 46.70 w/o O + 20.24 w/o Si + 4.92 w/o C + 0.83 w/o H	Ca O-16 Si C-12 H	0.008409 0.040431 0.009982 0.005874 0.011406
	II - Lead Mortar ρ = 2.5 (gm/cm^3) 2.4 w/o H + 3.3 w/o O + 5 w/o B + 15.2 w/o C + 73.6 w/o Pb	C-12 O-16 Pb B-10 H B-11	0.019073 0.003108 0.005349 0.001365 0.035887 0.005599
6	Blanket Mixture 3 v/o Graphite + 97 v/o Li_2O both at 60% density factor $\rho(Li_2O)$ = 2.013 (gm/cm^3), ρ(graphite) = 1.6 (gm/cm^3)	C-12 O-16 Li-6 Li-7	0.001444 0.023613 0.003504 0.043723
7	Graphite Reflector ρ(graphite) = 1.6 (gm/cm^3)	C-12	0.080226
8	Natural Quartz Window $\rho(SiO_2)$ = 2.64 (gm/cm^3)	O-16 Si	0.052928 0.026464

†Water-bound hydrogen cross sections were used

Table III

Neutron Group Structure and Associated Neutron Flux-to-Dose Factors

Group	Upper Edge (ev)	Midpoint Energy (ev)	(Rem/hr) per (n/(cm^2·sec))
1	1.491 + 07	1.420 + 07	2.273 - 04
2	1.349 + 07	1.285 + 07	2.083 - 04
3	1.221 + 07	1.163 + 07	2.083 - 04
4	1.105 + 07	1.052 + 07	2.083 - 04
5	1.000 + 07	9.524 + 06	1.471 - 04
6	9.048 + 06	8.617 + 06	1.471 - 04
7	8.187 + 06	6.837 + 06	1.471 - 04
8	5.488 + 06	4.250 + 06	1.526 - 04
9	3.011 + 06	1.709 + 06	1.250 - 04
10	4.076 + 05	2.054 + 05	9.259 - 05
11	3.354 + 03	1.677 + 03	3.550 - 06
12	4.140 - 01	2.070 - 01	4.456 - 06

Lower Edge: 1.000 - 04

Table IV

Element Identification

	Nuclide	ENDF/B Mat. No
1	C-12	1274
2	O-16	1276
3	Al-27	1193
4	Pb	1288
5	Li-6	1271
6	Li-7	1272
7	B-10	1273
8	B	1269
9	B-11	1160
10	Si	1194
11	Ca	1195

Table V Dimensions and Compositions of the Reactor Components

Region	Identification	Thickness (cm)	Volume (cm^3)	Material Composition
1	Inner Vacuum	-	-	Void
	Paraboloid Mirror			
2	Front	2.540	2.299 + 05	25 v/o H_2O + 75 v/o Al
3	Honeycomb Structure	50.800	5.288 + 06	Al
4	Rear	2.540	2.299 + 05	25 v/o H_2O + 75 v/o Al
	Flat Mirror			
5	Front	2.540	2.299 + 05	25 v/o H_2O + 75 v/o Al
6	Honeycomb Structure	50.800	2.288 + 06	Al
7	Rear	2.540	2.299 + 05	25 v/o H_2O + 75 v/o Al
8	Lead Acetate Tank Wall	0.635	1.441 + 05	Aluminum or Boral
	Lead Acetate + Boral Shield			
9	Zone 1	19.365	4.904 + 06	95 v/o $Pb(C_2H_3O_2)_2$ Solution
10	Zone 2	30.000	9.693 + 06	+ 5 v/o Boral
11	Zone 3	50.00	2.237 + 07	
12	Zone 4	50.000	2.939 + 07	
13	Zone 5	50.000	3.685 + 07	
14	Zone 6	50.000	4.509 + 07	
15	Paraboloid Mirror Shield Lining	0.635	1.122 + 05	Aluminum or Boral
	Paraboloid Mirror Shield			
16	Zone 1	19.365	3.942 + 06	
17	Zone 2	30.000	8.232 + 06	Ordinary Concrete
18	Zone 3	50.000	1.998 + 07	or
19	Zone 4	50.000	2.704 + 07	Lead Mortar
20	Zone 5	50.000	3.452 + 07	
21	Zone 6	50.000	4.278 + 07	
22	Blanket	64.500	4.878 + 06	3 v/o Graphite + 97 v/o Li_2O (both 60% d.f.)
23	Reflector	20.000	1.720 + 06	Graphite
24	Reactor Cavity Shield	360.000	5.158 + 07	Ordinary Concrete or Lead Mortar
25	Reactor Cavity Penetration Lining	1.319 to 2.217	3.724 + 05	Aluminum or Boral
26	Penetration Ring Shield	130.000	7.877 + 06	Ordinary Concrete or Lead Mortar
27	Flat Mirror Shield Lining	0.635	2.564 + 05	Aluminum or Boral
	Flat Mirror Shield			
28	Zone 1	19.365	8.846 + 06	Ordinary Concrete
29	Zone 2	30.000	1.792 + 07	or
30	Zone 3	50.000	4.235 + 07	Lead Mortar
31	Zone 4	50.000	5.642 + 07	
32	Zone 5	50.000	7.137 + 07	
33	Zone 6	50.000	8.788 + 07	
34	Quartz Window	50.000	2.262 + 06	SiO_2 (Natural Quartz)
	Duct Linings			
35	Paraboloid Mirror Cavity to Flat Mirror Cavity	0.635	8.572 + 04	Aluminum
36	Reactor Cavity to Paraboloid Mirror Cavity	0.635	1.443 + 05	or
37	Flat Mirror cavity to Quartz Window	0.635	1.384 + 05	Boral

Table VI

Comparison of Neutron Tracks for the Cases of
Aluminum and Boral as Duct Linings (2000 Histories)

Energy Group	Number of Neutron Tracks					
	Vacuum Region		Front of Paraboloid Mirror		Front of Flat Mirror	
	Aluminum	Boral	Aluminum	Boral	Aluminum	Boral
1	2129	2121	240	227	0	0
2	27	36	5	10	1	0
3	131	94	3	6	0	0
4	151	162	2	4	0	0
5	183	140	1	1	0	0
6	135	224	5	3	0	0
7	555	477	11	9	0	0
8	758	660	18	17	4	0
9	3159	2975	104	85	6	4
10	7492	7409	98	84	9	0
11	774	559	67	30	24	0
12	1096	3	380	5	140	0

Table VII

Comparison of Neutron Scalar Fluxes [n/(cm^2·sec)] in Different Reactor Components for the Cases of Aluminum or Boral as Laser Beam Duct Liners, and Ordinary Concrete or Lead Mortar as Shield Material

Case I: 2000 Histories Case II: 2000 Histories Case III: 8000 Histories

Reactor Components	Case I Aluminum Liner, Ordinary Concrete		Case II Boral Liner, Ordinary Concrete		Case III Boral Liner, Lead Mortar	
	Total Flux	Thermal Group Flux	Total Flux	Thermal Group Flux	Total Flux	Thermal Group Flux
Paraboloid Mirror						
Front	4.73 + 13	3.05 + 12	3.87 + 13	1.39 + 11	4.52 + 13	3.07 + 11
Honeycomb Structure	5.23 + 13	2.00 + 12	8.57 + 13	7.91 + 10	4.28 + 13	2.74 + 11
Rear	3.65 + 13	2.69 + 12	2.46 + 13	1.07 + 11	3.17 13	2.21 + 11
Flat Mirror						
Front	3.73 + 12	1.04 + 12	2.74 + 11	-	3.28 + 11	4.49 + 05
Honeycomb Structure	1.98 + 12	1.18 + 12	4.72 + 11	-	3.13 + 11	3.72 + 05
Rear	3.80 + 12	1.69 + 12	-	-	2.19 + 11	1.36 + 02
Blanket	5.01 + 14	5.19 + 10	5.05 + 14	4.68 + 10	4.91 + 14	2.33 + 10
Reflector	1.21 + 14	3.49 + 13	1.31 + 14	3.85 + 13	8.28 + 13	8.44 + 12
Reactor Cavity Shield	6.38 + 12	4.53 + 12	4.20 + 12	2.88 + 12	5.27 + 11	2.76 + 09
Ring Shield	7.58 + 11	6.57 + 11	3.34 + 11	2.28 + 10	3.47 + 10	7.58 + 07
Duct Linings						
Lead Acetate Tank	1.33 + 14	1.00 + 13	8.27 + 13	1.82 + 10	9.07 + 13	2.53 + 10
Reactor Cavity	1.06 + 14	1.81 + 13	6.64 + 13	1.03 + 11	6.33 + 13	2.28 + 09
Reactor Cavity to Paraboloic Mirror	1.54 + 13	9.03 + 12	3.13 + 12	3.12 + 10	4.00 + 12	2.79 + 09
Paraboloid Mirror Shield	5.96 + 13	1.66 + 13	2.79 + 13	7.82 + 10	3.36 + 13	6.57 + 09
Paraboloid Mirror to Flat Mirror	6.52 + 12	1.14 + 12	1.18 + 12	1.59 + 10	1.81 + 12	2.21 + 09
Flat Mirror Shield	9.16 + 12	4.55 + 12	3.31 + 12	1.00 + 09	1.39 + 12	1.12 + 04
Flat Mirror to Quartz Window	5.88 + 11	5.88 + 11	4.66 + 10	5.52 + 09	2.20 + 10	-
Quartz Window	6.11 + 10	4.89 + 10	-	-	8.93 + 10	-
Lead Acetate + Boral Shield						
Zone 1 (19.365 cm)	7.25 + 12	4.55 + 11	7.20 + 12	3.55 + 11	6.84 + 12	3.15 + 11
Zone 2 (30.000 cm)	1.27 + 12	5.83 + 10	1.19 + 12	6.74 + 10	1.28 + 12	7.03 + 10
Zone 3 (50.000 cm)	7.53 + 10	5.99 + 10	4.73 + 10	3.25 + 09	4.70 + 10	3.31 + 09
Paraboloid Mirror Shield						
Zone 1 (19.365 cm)	4.88 + 12	2.69 + 12	4.41 + 13	1.50 + 12	1.47 + 12	4.91 + 09
Zone 2 (30.000 cm)	3.50 + 12	2.52 + 12	1.48 + 12	1.11 + 12	2.68 + 11	3.82 + 08
Zone 3 (50.000 cm)	7.58 + 11	5.58 + 11	3.33 + 11	1.88 + 11	8.76 + 10	1.90 + 08
Flat Mirror Shield						
Zone 1 (19.365 cm)	1.06 + 12	8.32 + 11	1.86 + 11	3.73 + 10	5.07 + 10	2.51 + 08
Zone 2 (30.000 cm)	3.22 + 11	2.61 + 11	2.17 + 11	1.10 + 11	2.80 + 10	1.31 + 08
Zone 3 (50.000 cm)	1.24 + 11	9.71 + 10	4.19 + 10	1.84 + 10	1.20 + 10	2.11 + 07

Table VIII

Neutron Fluxes [n/(cm^2·sec)] in Different Reactor Components for Boral as a Penetration Lining and Lead Mortar as Shielding Material

Laser Energy: 150 MJ
Repetition Rate: 20 Hz
Number of Experiments: 20
Number of Histories per Experiment: 400

Reactor Components	14-Mev Group Flux	Thermal Group Flux	Total Flux*
Paraboloid Mirror			
Front	2.71 + 13	3.07 + 11	4.52 + 13 (0.07)
Honeycomb Structure	2.30 + 13	2.74 + 11	4.28 + 13 (0.05)
Rear	1.41 + 13	2.21 + 11	3.17 + 13 (0.08)
Flat Mirror			
Front	-	4.49 + 05†	3.28 + 11 (0.39)
Honeycomb Structure	-	3.72 + 05†	3.13 + 11 (0.71)
Rear	-	1.36 + 02	2.19 + 11 (0.44)
Blanket	4.61 + 13	2.33 + 10	4.91 + 14 (0.01)
Reflector	7.73 + 11	8.44 + 12	8.28 + 13 (0.03)
Reactor Cavity Shield	1.22 + 10	2.76 + 09	5.27 + 12 (0.03)
Ring Shield	5.93 + 09	7.58 + 07	3.47 + 10 (0.49)
Duct Linings (Boral)			
Lead Acetate Tank	2.90 + 13	2.53 + 10	9.07 + 13 (0.04)
Reactor Cavity	5.69 + 12	2.28 + 09	6.33 + 13 (0.02)
Reactor Cavity to Paraboloid Mirror	4.38 + 11	2.79 + 09	4.00 + 12 (0.13)
Paraboloid Mirror Shield	1.67 + 11	6.57 + 09	3.36 + 13 (0.11)
Paraboloid Mirror to Flat Mirror	-	2.21 + 09	1.81 + 12 (0.33)
Flat Mirror Shield	-	1.12 + 04	1.39 + 12 (0.36)
Flat Mirror to Quartz Window	-	-	2.20 + 10 (0.89)
Quartz Window	-	-	8.93 + 10 (0.90)
Lead Acetate + Boral Shield			
Zone 1	1.62 + 12	3.15 + 11	6.84 + 12 (0.04)
Zone 2	1.86 + 11	7.03 + 10	4.70 + 10 (0.28)
Zone 3	6.30 + 09	3.31 + 09	4.70 + 10 (0.28)
Paraboloid Mirror Shield			
Zone 1	1.57 + 10	4.91 + 09	1.47 + 12 (0.11)
Zone 2	2.91 + 09	3.82 + 08	2.68 + 11 (0.14)
Zone 3	7.20 + 09	1.90 + 08	8.76 + 10 (0.22)
Zone 4	6.43 + 09	5.44 + 07	2.11 + 10 (0.42)
Zone 5	1.12 + 09	3.60 + 07	1.46 + 10 (0.38)
Zone 6	-	1.15 + 07	3.82 + 09 (0.45)
Flat Mirror Shields			
Zone 1	-	2.51 + 08	5.07 + 10 (0.26)
Zone 2	-	1.31 + 08	2.80 + 10 (0.36)
Zone 3	-	2.11 + 07	1.20 + 10 (0.50)

†Track Length Estimator Estimate. All other estimates are from the Collision estimator.
*Values in brackets are fractional standard deviations.

Table IX

Comparison of Neutron Volumetric Heating Rates (Watts/cm^3)
In Different Reactor Components for the Cases of Aluminum or Boral
As Laser Beam Duct Liners, and Ordinary Concrete or Lead Mortar as Shield Material

Case I: 2000 Histories Case II: 2000 Histories Case III: 8000 Histories

Reactor Components	Case I Aluminum Liner Ordinary Concrete Shield	Case II Boral Liner Ordinary Concrete Shield	Case III Boral Liner Lead Mortar Shield
Paraboloid Mirror			
Front	1.24 + 00	1.29 + 00	1.44 + 00
Honeycomb Structure	2.85 - 02	2.56 - 02	3.14 - 02
Rear	8.92 - 01	6.70 - 01	8.68 - 01
Flat Mirror			
Front	1.42 - 02	2.19 - 03	2.04 - 03
Honeycomb Structure	8.41 - 05	2.73 - 05	2.93 - 06
Rear	4.75 - 03	-	9.23 - 04
Blanket	6.47 + 00	6.63 + 00	6.44 + 00
Reflector	2.40 - 01	2.54 - 01	2.23 - 01
Reactor Cavity Shield	6.62 - 03	4.66 - 03	2.04 - 02
Ring Shield	2.77 - 05	1.61 - 04	1.06 - 03
Duct Linings			
Lead Acetate Tank	1.66 + 00	1.59 + 00	1.97 + 00
Reactor Cavity	3.69 - 01	1.43 + 00	8.27 - 01
Paraboloid Cavity to Paraboloid Mirror	6.46 - 02	1.73 - 01	1.09 - 01
Paraboloid Mirror Shield	1.94 - 01	8.82 - 01	4.75 - 01
Paraboloid Mirror to Flat Mirror	1.36 - 02	1.45 - 01	4.47 - 02
Flat Mirror Shield	2.69 - 02	8.47 - 02	2.00 - 02
Flat Mirror to Quartz Window	8.83 - 04	3.12 - 02	1.51 - 04
Quartz Window	4.05 - 07	-	4.80 - 05
Lead Acetate + Boral Shield			
Zone 1 (19.365 cm)	3.25 - 01	3.30 - 01	3.12 - 01
Zone 2 (30.000 cm)	5.67 - 02	5.29 - 02	5.66 - 02
Zone 3 (50.000 cm)	4.05 - 03	1.85 - 03	2.02 - 03
Paraboloid Mirror Shield			
Zone 1 (19.365 cm)	9.98 - 03	2.17 - 02	4.99 - 02
Zone 2 (30.000 cm)	3.82 - 03	1.09 - 03	8.04 - 03
Zone 3 (50.000 cm)	7.98 - 04	9.11 - 04	2.68 - 03
Flat Mirror Shield			
Zone 1 (19.365 cm)	1.08 - 03	6.81 - 04	1.74 - 03
Zone 2 (30.000 cm)	1.61 - 04	6.59 - 02	9.72 - 04
Zone 3 (50.000 cm)	1.54 - 04	1.09 - 04	4.24 - 04

Table X

Spatial Dependences of the Neutron Heating Rates and Dose Rates in Different Reactor Components for Boral as the Duct Lining and Lead Mortar as the Shielding Material

Laser Energy: 150 MJ

Repetition Rate: 20 Hz

Number of Experiments: 20

Number of Histories per Experiment: 400

Reactor Components	Neutron Volumetric Heating Rates (Watts/cm^3)	Hypothetical Neutron Dose Rates (Rem/hr)
Paraboloid Mirror		
Front	1.44 + 00	7.92 + 09
Honeycomb Structure	3.14 - 02	7.33 + 09
Rear	8.68 - 01	5.10 + 09
Flat Mirror		
Front	2.04 - 03	2.79 + 07
Honeycomb Structure	2.93 - 06	2.90 + 06
Rear	9.23 - 04	1.32 + 07
Blanket	6.44 + 00	4.19 + 10
Reflector	2.23 - 01	3.14 + 09
Reactor Cavity Shield	2.04 - 02	4.22 + 07
Ring Shield	1.06 - 03	3.32 + 06
Penetration Linings (Boral)		
Lead Acetate Tank	1.97 + 00	1.30 + 10
Reactor Cavity	8.27 - 01	5.23 + 09
Reactor Cavity to Paraboloid Mirror	1.09 - 01	4.00 + 08
Paraboloid Mirror Shield	4.75 - 01	3.14 + 09
Paraboloid Mirror to Flat Mirror	4.47 - 02	2.16 + 08
Flat Mirror Shield	2.00 - 02	8.01 + 07
Flat Mirror to Quartz Window	1.51 - 04	2.03 + 05
Quartz Window	4.89 - 05	1.21 + 06
Lead Acetate + Boral Shield		
Zone 1	3.12 - 01	8.53 + 08
Zone 2	5.66 - 02	1.44 + 08
Zone 3	2.02 - 03	4.50 + 06
Paraboloid Mirror Shield		
Zone 1	4.99 - 02	1.35 + 08
Zone 2	8.04 - 03	2.65 + 07
Zone 3	2.68 - 03	8.47 + 06
Zone 4	7.57 - 04	2.74 + 06
Zone 5	4.91 - 04	1.44 + 06
Zone 6	1.29 - 04	1.93 + 05
Flat Mirror Shield		
Zone 1	1.74 - 03	3.50 + 06
Zone 2	9.72 - 04	3.01 + 06
Zone 3	4.24 - 04	1.35 + 06

Table XI

Spatial Dependences of the Radiation Damage Parameters in Different Reactor Components for Boral as a Penetration Lining and Lead Mortar as Shielding Material

Laser Energy: 150 MJ
Repetition Rate: 20 Hz
Number of Experiments: 20
Number of Histories per Experiment: 400

Reactor Components	Atomic Displacement Rates in Metal Components (Al) (dpa/sec)	Helium Gas Production Rates (appm/sec)	Hydrogen Gas Production Rates (appm/sec)
Paraboloid Mirror Aluminum			
Front	6.97 - 08	3.48 - 06	3.09 - 06
Honeycomb Structure	6.51 - 08	3.14 - 06	2.82 - 06
Rear	4.60 - 08	1.98 - 06	1.85 - 06
Flat Mirror Aluminum			
Front	2.67 - 10	1.88 - 12	5.86 - 10
Honeycomb Structure	8.65 - 11	1.88 - 12	-
Rear	1.33 - 10	-	1.32 - 11
Reactor Cavity Shield	n.a.†	3.69 - 07	2.21 - 09
Ring Shield	n.a.	1.45 - 08	2.09 - 10
Penetration Linings (Boral)			
Lead Acetate Tank	1.21 - 07	2.33 - 05	1.25 - 06
Reactor Cavity	5.38 - 08	1.37 - 05	3.62 - 07
Reactor Cavity to Paraboloid Mirror	3.82 - 09	2.52 - 06	2.03 - 08
Paraboloid Mirror Shield	3.16 - 08	1.00 - 05	1.30 - 07
Paraboloid Mirror to Flat Mirror	2.21 - 09	9.63 - 07	1.59 - 08
Flat Mirror Shield	9.42 - 10	5.00 - 07	1.92 - 09
Flat Mirror to Quartz Window	6.06 - 12	4.16 - 09	-
Quartz Window			
Aluminum in Boral in Lead Acetate			
Zone 1	7.96 - 09	3.87 - 05	9.06 - 08
Zone 2	1.38 - 09	8.56 - 06	1.46 - 08
Zone 3	4.38 - 11	4.00 - 07	4.41 - 10
Paraboloid Mirror Shield			
Zone 1	n.a.	7.68 - 07	6.97 - 09
Zone 2	n.a.	1.01 - 07	1.50 - 09
Zone 3	n.a.	3.74 - 08	4.67 - 10
Zone 4	n.a.	9.16 - 09	1.84 - 10
Zone 5	n.a.	6.62 - 09	9.73 - 11
Zone 6	n.a.	2.78 - 09	1.52 - 12
Flat Mirror Shield			
Zone 1	n.a.	3.14 - 08	1.81 - 10
Zone 2	n.a.	1.37 - 08	1.51 - 10
Zone 3	n.a.	5.40 - 09	9.04 - 11

Table XII

Computation Statistics for the Considered Cases

	Case I	Case II	Case III
Shield Material	Ordinary Concrete	Ordinary Concrete	Lead Mortar
Liner Material	Aluminum	Boral	Boral
Number of Experiments	20	20	20
Total Number of Histories	2000	2000	8000
Particles/experiment	100	100	400
CPU Time	28 min 36.10 sec	20 min 27.12 sec	50 min 38.42 sec
CPU Cost†	$25.74	$18.41	$45.58
Memory Usage	48.084	34.480	84.862
Memory Cost	$18.45	$13.23	$32.56
Particles Escaping	3	-	1
Escape Probability	3.328 - 04	-	1.118 - 04
Number of Scatterings	271951	189890	436657
Russian Roulette Triggering Weights			
In Liner	1.0 - 03	1.0 - 03	1.0 - 09
Penetration Shield	1.0 - 02	1.0 - 02	1.0 - 05
Reactor Cavity	1.0 - 02	1.0 - 02	1.0 - 03
Total Cost	$44.19	$31.64	$78.14

†Based on weekend rates on the UW-UNIVAC-1110